Air Force Institute of Technology

AFIT Scholar

Theses and Dissertations

Student Graduate Works

10-11-2007

Time Resolution of Collapse Events During the Progation of Ultraviolet Filaaments

Teresa J. Fondren

Follow this and additional works at: https://scholar.afit.edu/etd

Part of the Plasma and Beam Physics Commons

Recommended Citation

Fondren, Teresa J., "Time Resolution of Collapse Events During the Progation of Ultraviolet Filaaments" (2007). *Theses and Dissertations*. 2715.
https://scholar.afit.edu/etd/2715

This Thesis is brought to you for free and open access by the Student Graduate Works at AFIT Scholar. It has been accepted for inclusion in Theses and Dissertations by an authorized administrator of AFIT Scholar. For more information, please contact richard.mansfield@afit.edu.

www.manaraa.com

Time Resolution of Collapse Events
During the Propagation of
Ultraviolet Light Filaments

THESIS

Teresa J. Fondren, First Lieutenant, USAF

AFIT/GAP/ENP/08-M03

DEPARTMENT OF THE AIR FORCE
AIR UNIVERSITY

AIR FORCE INSTITUTE OF TECHNOLOGY

Wright-Patterson Air Force Base, Ohio

APPROVED FOR PUBLIC RELEASE; DISTRIBUTION UNLIMITED.

المنارة للاستشارات
www.manaraa.com

The views expressed in this thesis are those of the author and do not reflect the official policy or position of the United States Air Force, Department of Defense, or the United States Government.

المنارة للاستشارات
www.manaraa.com

AFIT/GAP/ENP/08-M03

Time Resolution of Collapse Events During the Propagation of Ultraviolet Light Filaments

THESIS

Presented to the Faculty

Department of Engineering Physics

Graduate School of Engineering and Management

Air Force Institute of Technology

Air University

Air Education and Training Command

In Partial Fulfillment of the Requirements for the

Degree of Master of Science in Applied Physics

Teresa J. Fondren, B.S. in Physics and in Mathematics

First Lieutenant, USAF

March 2008

APPROVED FOR PUBLIC RELEASE; DISTRIBUTION UNLIMITED.

المنارة للاستشارات

www.manaraa.com

AFIT/GAP/ENP/08-M03

Time Resolution of Collapse Events During the Propagation of Ultraviolet Light Filaments

Teresa J. Fondren, Bachelor of Science in Physics and in Mathematics
First Lieutenant, USAF

Approved:

Thomas Niday (Chairman)	11 Oct 07 Date
David Weeks (Member)	11 Oct 07 Date
Matthew Bohn (Member)	11 Oct 07 Date

AFIT/GAP/ENP/08-M03

Abstract

Long distance propagation, or filamentation, of short, intense laser pulses is suggested to be possible through the balance of two effects: self-focusing, when a nonlinear index of refraction of air is induced by high intensities, and de-focusing, due to the plasma created by the pulse. Applications for filamentation include areas such as remote sensing and directed energy. A split-step spectral propagation simulation is used to model the behavior of a high intensity ultraviolet laser pulse propagating through air. Convergence of femtosecond duration collapses that form on the leading edge of the pulse in the time domain is achieved with an increase in the multi-photon ionization coefficient. Through an analysis of the relative sizes of each term in the propagation equation, a lack of plasma present at the leading edge of the pulse is found to cause these collapses. Results for a more recent value of the electron-positive ion recombination rate are compared to results from a higher value used in previous works. A linear stability analysis shows inherent instability of the pulses in all cases. The inclusion of group velocity dispersion is shown to increase stability at high temporal frequencies except at zero spatial frequencies. A run similar to an experiment that produced UV filamentation is shown to propagate 70 cm without exceeding numerical limitations.

المنارة للاستشارات
www.manaraa.com

Acknowledgements

First and foremost, I want to thank God for giving me the opportunity, ability, desire, and perseverance to acquire this advanced degree. I also need to thank my advisor, Maj Thomas Niday, for all of his suggestions, guidance, and patience during this thesis effort, as well as giving up his computer while I needed it for this work. I would also like to thank Dr. Hengehold for his willingness to work with me in accelerating my program so that I could rejoin my husband sooner. I thank my parents for their amazing encouragement and belief in me. Finally, my husband deserves my sincerest gratitude for helping me through this academic experience despite the hundreds of miles separating us.

Teresa J. Fondren

المنارة للاستشارات
www.manaraa.com

Table of Contents

Page

Abstract iv

Acknowledgements v

List of Figures viii

List of Tables x

I. Introduction 1
- Motivation 1
- Problem Statement 6
- Previous Work 8
- Objectives and Methods 13

II. Theory Review 16
- Propagation Equation 16
- Simplifying Assumptions 18
- Self-Focusing and Filamentation 20
- Group Velocity Dispersion 23
- Theoretical Summary 26

III. Methodology 28
- Physical and Numerical Parameters 28
- Numerical Methods 30
- Limitations of Numerical Methods 37
- Summary of Methodology 41

IV. Results and Analysis 43
- Time Convergence 43
- Details of Collapse Events 53
- Stability Analysis 54
- Propagation Term Values 66
- Experimental Verification 73
- Summary 76

V. Conclusions and Suggestions 84
- Research Conclusions 84
- Impact of Research 87
- Suggestions for Further Research 89

المنارة للاستشارات
www.manaraa.com

Page

Bibliography 95

Vita 98

المنارة للاستشارات

www.manaraa.com

List of Figures

Figure		Page
1.1.	Propagation of a finite duration pulse	8
1.2.	Muller's time convergence plots.	11
1.3.	Muller's time convergence plots with increased MPI Coefficient	12
2.1.	X-Wave Example	23
3.1.	Full 3D view of pulse propagation and fluence profile A	33
3.2.	Full 3D view of pulse propagation and fluence profile B	34
3.3.	Full 3D view of pulse propagation and fluence profile C	35
3.4.	Frequency representation of propagating pulse	40
4.1.	Time Convergence with increased MPI coefficient.	45
4.2.	Time Convergence with GVD.	46
4.3.	Time convergence with old recombination rate.	48
4.4.	Time convergence with new recombination rate.	49
4.5.	Comparison of recombination rates.	50
4.6.	Plasma Density of both recombination rates at 12.5 cm	51
4.7.	Plasma Density of both recombination rates at 25 cm	52
4.8.	Niday's steady state solution	55
4.9.	Growth rate vs. $\bar{k}_\perp$ and Ω without GVD included	60
4.10.	Growth rate vs. $\bar{k}_\perp$ and Ω, without GVD, with α_n, and with a higher MPI coefficient	60
4.11.	Comparison of growth rate with and without GVD at high temporal frequencies	61
4.12.	Comparison of growth rate with and without GVD at high temporal frequencies with new recombination rate and high MPI coefficient	62
4.13.	Growth rate vs. Ω, when $\bar{k}_\perp = 0$.	64
4.14.	Growth rate vs. Ω, when $\bar{k}_\perp \to \infty$.	65

المنارة للاستشارات
www.manaraa.com

Figure Page

4.15. Propagation equation term values at 2.5 cm 68

4.16. Propagation equation term values at 12.5 cm 69

4.17. Propagation equation term values at 50 cm 70

4.18. GVD term 73

4.19. Perturbations caused by the GVD parameter. 74

4.20. Plasma propagation terms 75

4.21. Gaussian pulse with k-space representation and fluence profile at 1.25 cm 77

4.22. Gaussian pulse with k-space representation and fluence profile at 15 cm 78

4.23. Gaussian pulse with k-space representation and fluence profile at 30 cm 79

4.24. Gaussian pulse with k-space representation and fluence profile at 50 cm 80

4.25. Gaussian pulse with k-space representation and fluence profile at 70 cm 81

4.26. Time slice of Gaussian pulse propagation 82

المنارة للاستشارات
www.manaraa.com

List of Tables

Table Page

3.1. Parameters for UV pulse simulations 29

المنارة للاستشارات
www.manaraa.com

Time Resolution of Collapse Events During the Propagation of Ultraviolet Light Filaments

I. Introduction

Motivation

Dedicated research is currently being done on the long distance propagation of intense ultrashort laser pulses through the atmosphere. Applications for this include remote sensing [1–3], directed energy [4, 5], and laser induced lightning [6, 7]. All of these applications are especially interesting to the military for protecting forces from harmful environmental effects, shielding them from enemy sensing capabilities, allowing them access to information that has been previously unattainable, and inflicting damage to enemy forces. In order for these applications to be optimized, two things are required. First, to further the effective reach, the range of propagation through atmospheric phenomena such as rain, clouds, and dust particles needs to increase. Second, to be most effective, more power needs to be transferred with the pulses all the way to the target [8].

Long propagation distances of laser pulses have been demonstrated in both the infrared (IR) and ultraviolet (UV) wavelength ranges due to filamentation of the pulses [9–11]. This thesis will use a definition of filamentation or filaments from Couairon:

المنارة للاستشارات
www.manaraa.com

> Filamentation [refers to] a dynamic structure with an intense core that is able to propagate over extended distances much larger than the typical diffraction length while keeping a narrow beam size without the help of any external guiding mechanism [12].

Another, stricter definition is also used in the literature that refers to filaments as only the part of the beam propagation where the pulse generates a column of weakly ionized plasma in its wake due to a sufficiently high intensity in its core.

Filamentation is induced when the power of a pulsed beam is above a certain critical power that is proportional to the square of the wavelength. The high power initiates a nonlinear effect known as the optical Kerr effect which causes self-focusing of the laser pulse. The Kerr effect introduces an intensity dependent refractive index when the pulse power is equal to or greater than the critical power, creating an effective focusing lens in the refractive profile of the air [8]. While focusing, the pulse eventually reaches a high intensity as it overcomes diffraction. This causes ionization of the air around it, forming a surrounding plasma. The plasma, in turn, absorbs photons from the pulse and changes the index of refraction of air, resulting in a decrease in pulse intensity and an effective negative lens that defocuses the pulse. Studies have suggested that balancing these focusing-defocusing effects will allow propagation over long distances on the order of several Rayleigh ranges or further (up to kilometers [13]), possibly even through atmospheric obscurants [2, 3, 9–12, 14].

Much of the research involving long-distance propagation of light filaments in air due to self-focusing deals with wavelengths in the IR range (>750 nm). A

المنارة للاستشارات
www.manaraa.com

main attraction to this wavelength is due to an extra effect called ultra-broadband radiation that light filaments of these wavelengths can generate. This radiation emits a white-light super-continuum range of wavelengths from 500 nm to 1200 nm, which can be used to remotely monitor trace gases and aerosols in the air [1, 15]. By directing such a continuum of wavelengths at a target, a wide range of aerosols could be detected through observing the absorption of certain wavelengths from the continuum. Early warning systems for bioterrorist threats could be achieved based on selective remote sensing of aerosols with the ultra-broadband radiation induced from IR filamentation since aerosols can be used as carriers for toxic species to be absorbed into the lungs. Extending the Lidar (light detection and ranging) technique with nonlinear and multispectral measurements, the white-light super-continuum effect could allow the retrieval of the abundance, particle size, and refractive index of a diverse set of aerosol particles. Previously, remote identification of these aerosols was extremely difficult due to the variety of their size, shape, and composition [16].

Although this white light phenomenon is not reported for UV filaments [9], using wavelengths of 10-400 nm has other wanted characteristics for filamentation. Since the critical power needed for filamentation is proportional to the square of the wavelength, UV filaments require a much lower peak power, with an on-axis intensity on the order of 1 TW/cm^2, in comparison to 100 TW/cm^2 for IR [5,17]. This results in three possible advantages:

المنارة للاستشارات
www.manaraa.com

- Longer UV pulses can be used while still being able to have enough power for filamentation. These longer pulses should be able to travel longer distances since the filaments can contain more energy [18].
- Many of the higher order nonlinear effects important for IR ultra-short pulses can be neglected for longer UV pulses.
- The focus-defocus balance for long distance propagation could become solely intensity dependent allowing the increase of pulsewidth to increase filament energies [5].

These potential advantages of UV pulses create a demand for more research involving UV filaments. There is a need to better understand the physics behind UV filament propagation in order to exploit its usefulness.

One of the most interesting applications of this filamentation is in the area of self-healing. Work has been done to investigate the effects of atmospheric obscurants on the long distance propagation of laser pulses. Skupin et al. [14] were able to theoretically show that single filaments can survive interaction with obscurants sized up to two-thirds that of the filament diameter. This agrees with the experimental data of Courvoisier et al [2]. The durability of the filaments is due to the ability of some beam components that are kept untouched after collision with the obscurant to refocus and continue with a power above critical. Through self-focusing again onto the beam axis, these components are able to replenish the filament within a few centimeters. In other words, instabilities in

المنارة للاستشارات
www.manaraa.com

the filament, caused by the high powers needed to overcome the critical power required for filamentation, allow it to split into several smaller filaments when it encounters an obscurant. Afterwards, the filaments recombine or self-heal and continue along the original path with only a 10-15% loss in power [3]. This could allow long range sensing to be done through thin clouds and other obscurants. This ability to propagate through adverse weather would be invaluable for military remote sensing applications.

Laser induced lightning is another application of filamentation. It is based on the plasma wake left by the laser as the filaments propagate. UV laser pulses, with their smaller wavelength, are better suited for this application since they can produce a longer conducting plasma column than IR laser pulses [12]. The idea is to use this plasma channel created by the filamentation of a high-powered short-pulsed laser to trigger and guide a high-voltage discharge such as lightning [6, 16, 19]. By controlling where and how lightning strikes in a storm, sensitive sites such as electrical installations or airports could be protected from direct strikes and electromagnetic perturbations. Rodriguez et al. were able to demonstrate the complete guiding of a discharge produced at the high-voltage facility of the Technical University of Berlin [20].

This same idea could be used for application in directed energy. Instead of lightning being induced and guided, the plasma channel created by the laser would guide a purposed electrical discharge directly to a target to either destroy

المنارة للاستشارات
www.manaraa.com

it or limit its capabilities. In reference [4], Davis et al. suggest a four-step process. First, a laser creates a plasma channel that has low conductivity all the way to the target. Second, the conductivity of the channel increases by several orders of magnitude as a leader is propagated down it. Third, a return stroke increases the channel conductivity even further, allowing swift and efficient delivery of energy. Last, the ohmic dissipation along the line drives the conductivity up even further with pulse delivery. This four-step process could allow military forces to send a low impedance lightning-like arc strike to destroy a target.

There are many other potential applications for light filamentation such as generation of single cycle pulses and high order harmonics, laser induced breakdown spectroscopy (LIBS), power supply for high speed electric vehicles, and even advances in propulsion. A detailed summary of these applications and the research done up to this point in the area of filamentation is presented by Couairon and Mysyrowicz in reference [12].

Problem Statement

Although there has been a thorough amount of research concerning IR light filaments and much of the science is understood and can be reproduced numerically and experimentally, the details of UV filamentation are still debated. In order to tap into the benefits of using UV pulses, a better understanding of what is physically happening in the long distance propagation of UV filaments is needed. Many studies [5, 8, 9, 11, 21–23] have investigated the stability of UV pulses with

المنارة للاستشارات
www.manaraa.com

respect to the balancing of self-focusing and diffraction terms in the propagation equation. There have been experimental results showing propagation of UV pulses to distances up to twelve meters [5]. The question remaining and being discussed in papers on the subject of UV filamentation is *how* these filaments are able to travel these distances with stability.

Currently, long pulse models of UV filamentation exhibit spatial and temporal instabilities within the pulse, causing it to breakup, possibly limiting its propagation distance [21,23]. In Niday's long pulse propagation results, the pulses form collapse events on the leading edge of the pulse. Figure 1.1 is taken from Niday's dissertation [21] and shows the development of collapse events on the leading edge of the pulse and the instabilities exhibited as it propagates. These peaks are three magnitudes of order shorter in time than the original pulse, thus making it difficult to numerically model the whole pulse while having enough resolution to be able to understand the details of the collapses. Propagation to distances of about one meter with this code, in some cases, creates an overflow of the numerical parameters where the computational area (spatial grid) is not fine enough. In the spatial frequency representation, non-zero values start to exist at the boundaries that are then wrapped around to the opposite edge causing non-physical results that lead to the disintegration of the pulse starting from the trailing edge. Higher computing power that can keep track of a larger grid or better coding that can allow for a larger grid with the same amount of computing power is needed to in-

المنارة للاستشارات
www.manaraa.com

vestigate the causes of these leading edge collapse events and be sure to eliminate effects caused by numerical grid overflow. Understanding these details will lead to a better understanding of the interaction between focusing and de-focusing terms in the propagation equation, opening the door to applications of long distance propagation of UV pulses.

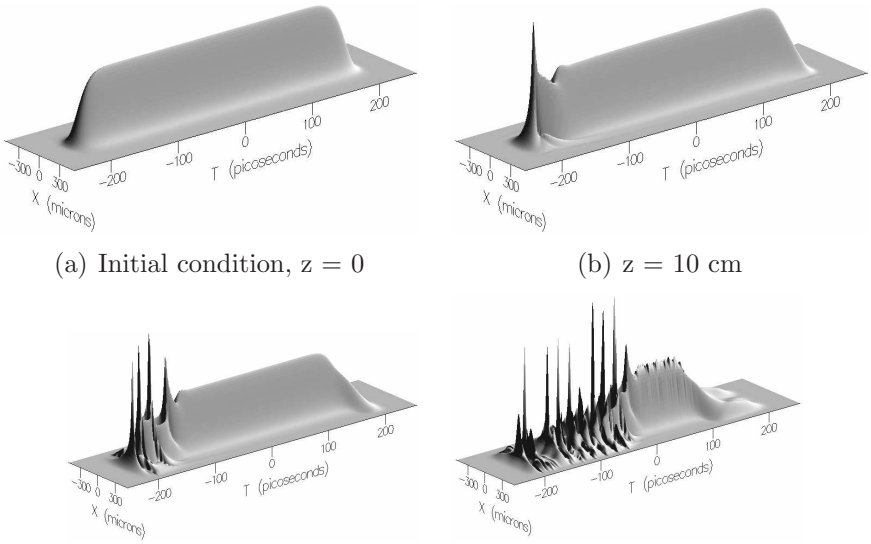

(a) Initial condition, z = 0

(b) z = 10 cm

(c) z = 25 cm

(d) z = 75 cm

Figure 1.1: Propagation of a finite duration pulse (400 ps) taken from reference [21]. Note the beginning of the collapse of the leading edge of the pulse and the series of collapse events that consumes the pulse as it continues to propagate.

Previous Work

As mentioned above, Niday created a code in FORTRAN that models the propagation of a relatively long pulse (on the order of picoseconds) through air at high powers, taking into account nonlinear terms that induce self-focusing [21]. An example of the collapse events and then pulse consumption resulting from the propagation of a pulse in his code is presented in Figure 1.1.

المنارة للاستشارات
www.manaraa.com

Niday came to several conclusions during his investigation of the long distance propagation of UV pulses. His first conclusion was that the collapses on the leading edge of the pulse are caused by the transient shape of that edge. He chose a supergaussian shape so that in its middle, where it is flat, it emulates a steady state solution for which he had solved. But the transient edge shape does not match the steady state solution, thus causing the collapses. He suggested that the collapses are due to the pulse trying to move toward a steady state solution. He also proposed that the collapses consumed the pulse at a linear rate, so the collapses do not develop faster as more of the pulse is consumed. He was not, however, able to show convergence in time of these collapse peaks due to limited grid size and numerical parameters. A key component to his research is linear stability analysis. Without considering losses, he found that all spatial and temporal frequencies are able to grow, thus causing instability in the propagation of the pulse.

Muller continued Niday's work, investigating four areas in further detail [8]. First, he varied the numerical parameters of the propagation model in order to find the optimal combination of computational efficiency and resolution of pulse characteristics while striving for convergence. He concluded that a spatial grid (number of data points in the x and y directions) of 128×128 elements spaced 8 μm apart and a propagation step in the z direction of 0.5 mm produced spatial convergence. In the time domain, because of computational limitations, he sug-

المنارة للاستشارات
www.manaraa.com

gested a ratio of time step to pulse duration of 1:100 for a supergaussian profile and 1:20 for a Gaussian on a grid of 512 elements. This, however, did not lead to a fully converged result (see Figure 1.2). By increasing the multi-photon ionization (MPI) coefficient $\beta^{(K)}$ by a factor of 10 and decreasing the time step to pulse duration ratio, he was able to approach convergence for collapses of a pulse with an initial peak power of 250 MW (Figure 1.3). In this work, time convergence of the pulse collapses is produced using a more powerful computer than what was available to Muller.

Second, Muller studied the effects of initial power on the collapse of the pulse. He determined that higher initial power increased the number of collapses that occurred, but did not affect the rate at which the entire pulse was consumed by these collapse events [8]. It should be noted that he did not have complete convergence when discovering this result.

Third, Muller did a detailed study on the relationship of the plasma to the collapse events. He concluded that they are very closely related. After the intensity of the pulse reaches a certain level due to self-focusing, it begins to ionize the surrounding air, thus generating plasma. Once enough plasma is generated, the pulse begins to defocus, losing its intensity and stopping the generation of plasma. As the plasma decays, self-focusing begins to dominate once again, creating another collapse event. He also claimed that the nominal value of the electron-positive ion recombination coefficient α was 1.1×10^{-12} m^3/s since only

المنارة للاستشارات
www.manaraa.com

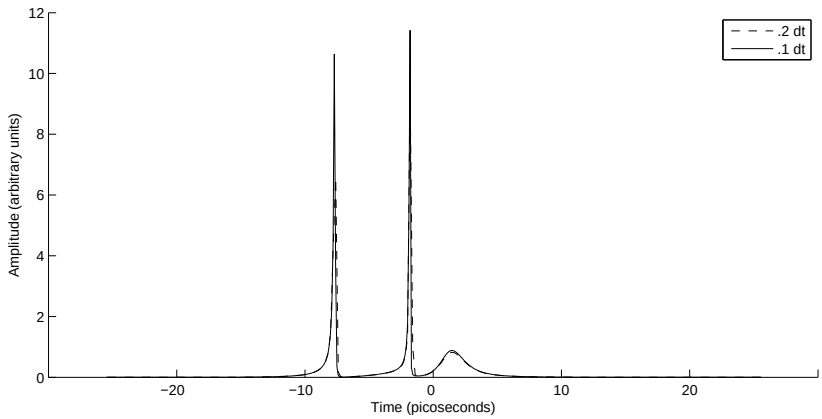

(a)

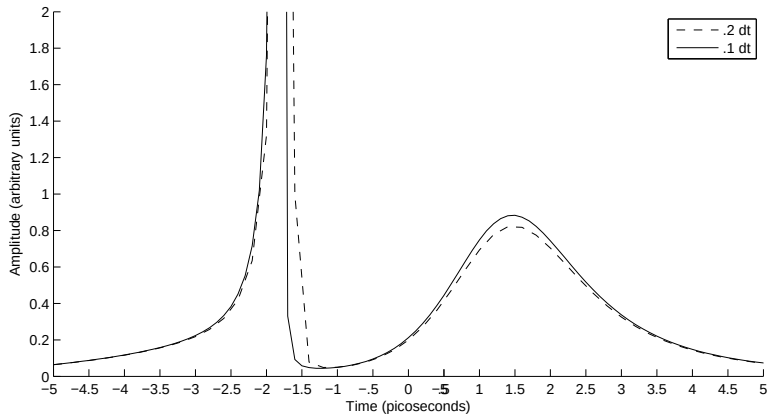

(b)

Figure 1.2: Paul Muller's plot of a 500 MW, 20 ps pulse after propagating 25 cm for two different values of $\triangle t$. Plot (b) represents a zoomed in area of (a), and the scaling of the plot has cut off the top of the first peak.

المنارة للاستشارات
www.manaraa.com

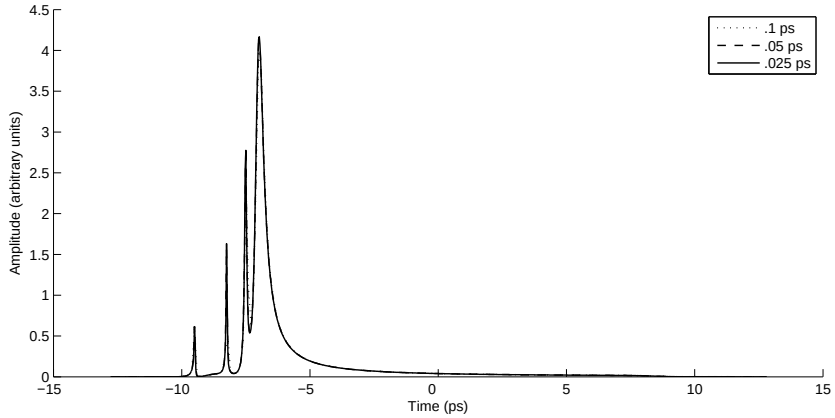

(a)

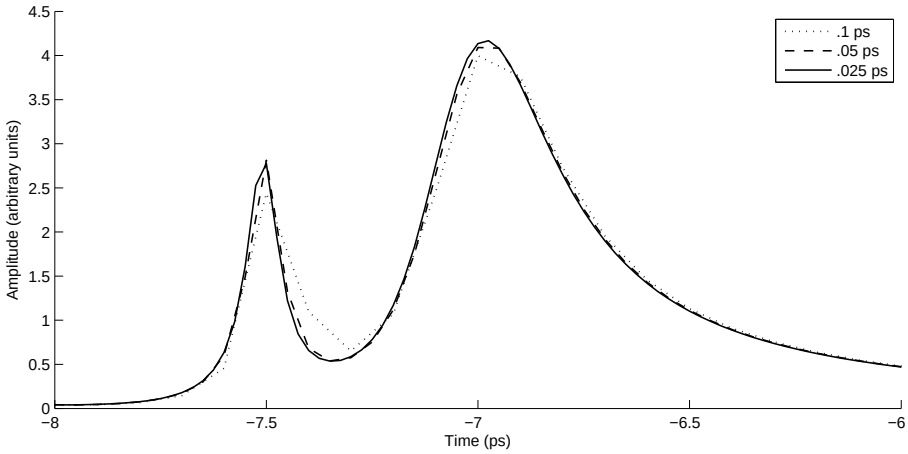

(b)

Figure 1.3: Paul Muller's plot of a 250 MW, 20 ps pulse with $\beta^{(K)}$ increased by a factor of 10. Plot (b) represents a zoomed in area of (a).

المنارة للاستشارات
www.manaraa.com

slight adjustments caused the model to fail. This was discovered to be incorrect by Chalus, however, who suggested a much smaller value [24]. This new value of 1.3×10^{-14} m^3/s is incorporated into this study. Muller also suggested that collapse events produced on the trailing edge of a pulse are due to an overflow of the model's grid in the spatial frequency domain. Care is given in this study to alleviate this numerical error.

Finally, Muller added a group velocity dispersion (GVD) term to the propagation code to investigate much smaller pulse durations. He determined that the GVD term did not affect pulses of duration longer than 100 fs and that even with GVD taken into consideration, 10 fs pulses also collapsed without propagating a long distance. This work will reproduce code to account for GVD and incorporate it in the study of the collapse events even for pulses longer than 100 fs because his results were obtained without full convergence of the collapse events. Considering the collapse events are on the order of femtoseconds, GVD might play a role in their development.

Objectives and Methods

This thesis continues the work of Niday, focusing specifically on Muller's efforts to achieve time convergence of the collapse events. By updating the FORTRAN code authored by Niday, the pulse duration is decreased from Niday's 400 ps pulses down to 10 ps pulses to allow for a decrease in the time grid spacing with a reasonable increase in the number of grid points. This provides enough

المنارة للاستشارات
www.manaraa.com

resolution to validate the shape of the collapse events up to a propagation distance of ~ 50 cm. Analysis of the time convergence and shape of these collapses is done with the help of Matlab® code that Muller created. In order to understand more about what is causing these collapse events and how they are forming, a detailed analysis of the individual terms in the propagation equation is presented with the help of Mathematica®. All of this is done on a dedicated workstation with two dual-core processors, AMD Opteron 275 with 16 GB RAM that was procured prior to the start of this project.

An investigation of the individual terms in the propagation equation is done to include the MPI coefficient and its role in shaping the collapse events. In Muller's work, increasing this MPI parameter artificially led to better convergence of the collapse events. An explanation for this result is given and discussed. Also, an updated value of the electron-positive ion recombination coefficient α in the plasma calculations is employed. Chalus suggests that previous literature has been using a value two orders of magnitude higher than the correct value of 1.3×10^{-14} m^3/s [24]. The difference this new value makes on the behavior of the pulse propagation is presented along with an explanation. Also, the role that GVD plays in the development of collapse events is detailed to include its small value relative to the other propagation terms and its effect on the stability analysis.

An expanded stability analysis based on the analysis done by Niday in reference [21, 23] is conducted. The analysis includes group velocity dispersion effects

المنارة للاستشارات
www.manaraa.com

and takes into account how losses compare to the growth rate. The analysis is done with various combinations of the different values for the recombination rate and multi-photon ionization coefficient. It is determined that the inclusion of GVD to the diffraction and Kerr terms that Niday used leads to a slower growth rate for high temporal frequencies, except at zero spatial frequencies GVD causes the growth rate to be non-zero. Although a full loss analysis is not conducted, the losses are found to be insignificant compared to the growth rate, except at high intensities on the order of 10^{17} W/m^2.

المنارة للاستشارات
www.manaraa.com

II. Theory Review

This chapter will give the reader a foundation in the physics needed to understand this research. It starts with the basic principles that govern the propagation of light, goes on to address the individual terms of the propagation equation, and then goes into further detail on the most important terms for the interests of this thesis.

Propagation Equation

Understanding the propagation of a laser beam or pulse through air begins with the Maxwell wave equation,

$$\nabla^2 E - \frac{n_0^2}{c^2}\frac{\partial^2 E}{\partial t^2} = \frac{1}{\epsilon_0 c^2}\frac{\partial^2 P_{NL}}{\partial t^2}, \tag{2.1}$$

where n_0 is the linear refractive index, ϵ_0 is the permittivity of free space, μ_0 is the permeability of free space, and $c^2 = 1/(\epsilon_0\mu_0)$. P_{NL} is the nonlinear polarization and can include all nonlinear effects, but may be written simply as $\epsilon_0\chi^{(3)}|\mathcal{E}|^2 E$ for self-focusing. $\chi^{(3)}$ is equal to $2n_0n_2$, where n_2 is the self-focusing index. $\mathcal{E}$ is a complex amplitude of the slowly varying envelope of the electric field and has units that are defined such that the irradiance, or what we will call intensity, $|\mathcal{E}|^2$, has units of W/m^2. For a wave propagating along the z-axis, the electric field E

المنارة للاستشارات
www.manaraa.com

is represented by:

$$E\left(x,y,z,t\right)=\frac{1}{2}\mathcal{E}\left(x,y,z,t\right)e^{i(kz-\omega t)}+c.c. \tag{2.2}$$

with ω being the angular frequency and with $k=n_0\omega/c$. Using equations (2.1) and (2.2) and the nonlinear polarization terms and effects of plasma generation that Niday [21, 23], Schwarz and Diels [11], and Muller [8] use, one can obtain

$$\begin{aligned}\frac{\partial\mathcal{E}}{\partial z}=\frac{i}{2k}\nabla_{\perp}^{2}\mathcal{E}-\frac{ik''}{2}\frac{\partial^{2}\mathcal{E}}{\partial t^{2}}-\frac{\beta^{(K)}}{2}|\mathcal{E}|^{2K-2}\mathcal{E}-\frac{\sigma}{2}\left(1+i\omega\tau\right)\rho\mathcal{E}\\ +ik_0n_2(1-f)|\mathcal{E}|^2\mathcal{E}+ik_0n_2f\left[\int_{-\infty}^{\infty}dt'R(t-t')|\mathcal{E}(t')|^2\right]\mathcal{E}\end{aligned} \tag{2.3}$$

to describe how $\mathcal{E}$ changes as a function of the propagation distance z. The first term on the right hand side of the equation represents transverse diffraction. It is followed by a term expressing group velocity dispersion (GVD) where k'' represents the second order derivative of the wave number k with respect to ω. The third term describes multi-photon ionization where $\beta^{(K)}$ is the coefficient for MPI of the Kth order. In the case of UV propagation in air, $K=3$ for $\lambda=248$ nm because three photons with energy of approximately 5 eV are required to ionize one O_2 molecule with ionization energy of approximately 13.6 eV, therefore generating a plasma. The fourth term is a plasma term where σ is the cross section for inverse bremsstrahlung, ω is the optical reference frequency of the light, τ is the electron collision time, and ρ is the electron plasma density. The last two terms represent

المنارة للاستشارات
www.manaraa.com

self-focusing and the Raman effect, where f is the fraction of the Kerr effect which is not instantaneous, but delayed due to stimulated molecular Raman scattering.

Simplifying Assumptions

To be able to model the behavior of a propagating pulse, taking into account the self-focusing terms needed to produce long distance propagation, one can make certain simplifying assumptions in order to accommodate the time and computational abilities at hand. In equation (2.3), we neglect the last term describing the Raman effect according to Niday [21]. His investigation showed that for UV pulses on the order of picoseconds the Raman contribution to n_2 was found to be insignificant due to the lack of spectral broadening before the pulses ionize. Niday's conclusions on Raman scattering were founded on the work of Peñano et al [25]. Therefore, equation (2.3) reduces to

$$\frac{\partial \mathcal{E}}{\partial z} = \frac{i}{2k} \bigtriangledown_{\perp}^{2} \mathcal{E} - \frac{ik''}{2} \frac{\partial^2 \mathcal{E}}{\partial t^2} - \frac{\beta^{(K)}}{2} |\mathcal{E}|^{2K-2} \mathcal{E} - \frac{\sigma}{2} (1 + i\omega\tau) \rho \mathcal{E} + ik_0 n_2 |\mathcal{E}|^2 \mathcal{E}. \quad (2.4)$$

In order to evaluate the plasma term in the above equation, we describe the electron plasma density ρ by

$$\frac{\partial \rho}{\partial t} = C\rho|\mathcal{E}|^2 + \frac{\beta^{(K)}|\mathcal{E}|^{2K}}{K\hbar\omega} - \alpha\rho^2 + D \bigtriangledown_{\perp}^{2} \rho, \quad (2.5)$$

المنارة للاستشارات
www.manaraa.com

where C is the avalanche ionization coefficient, α is the electron-positive ion recombination coefficient, and D is the diffusion strength. In previous literature a value of 1.1×10^{-12} m^3/s was used for α [5, 8, 13, 21, 23]. This value was also used for the first half of this research, but was changed to 1.3×10^{-14} m^3/s to agree with the new value that Chalus presents in reference [24]. We assume no diffusion, so $D = 0$, and the pulse durations are short enough to neglect the avalanche ionization so we can also set $C = 0$ [11]. Niday, Muller, and Schwarz and Diels [8, 11, 21, 23] use a steady state solution found by setting $\frac{\partial\rho}{\partial t} = 0$ to express the plasma density as a power of intensity for their two dimensional code. We, however, only employ Niday's 3D code which must solve the differential equation (2.5) for each propagation step. A detailed analysis of the range needed for these approximations is provided by Zhang [17], which says that for steady state to apply, the UV pulses must be at least a few tens of picoseconds long, and in order to neglect avalanche ionization they must be shorter than several nanoseconds. Since we are dealing with ps pulses, the equation that must be solved in order to describe the plasma density becomes

$$\frac{\partial\rho}{\partial t} = \frac{\beta^{(K)}|\mathcal{E}|^{2K}}{K\hbar\omega} - \alpha\rho^2. \tag{2.6}$$

For a 248 nm pulse propagating in air, $K = 3$, and the value for $\beta^{(3)}$ is 3.9×10^{-34} m^3/W^2. This value is used in many other references as well [5, 8, 11, 13, 21, 23]. However, different values are also employed in the literature [17, 22] ranging from

المنارة للاستشارات
www.manaraa.com

9.55×10^{-34} to 1.0×10^{-31}. This throws the exact value of the MPI coefficient into question. Therefore, we will investigate what increasing this value by an order of magnitude does to the propagation of the pulse.

Another effect not present in equation (2.3) is Rayleigh scattering. According to reference [17], after approximately 400-500 meters of propagation, Rayleigh scattering begins to significantly affect the filament propagation. The model used by Niday and Muller has not yet been able to stably propagate to a distance of this magnitude, but it is worth mentioning.

Self-Focusing and Filamentation

A major factor in filamentation is the self-focusing Kerr effect. The refractive index is not only frequency dependent as is addressed when dealing with GVD in the following section, but it is also intensity dependent according to $n = n_0 + n_2 I(x, y, t)$ [12]. As the intensity increases, the nonlinear Kerr index n_2 has a greater effect on the refractive index. In a normal Gaussian pulse, the intensity is greatest in the center and declines radially outward. This, in effect, creates a virtual lens that focuses the pulse. This self-focusing can overcome diffraction once the peak power of the pulse reaches a critical power given by

$$P_{cr} = \frac{\lambda^2}{2\pi n_0 n_2}, \tag{2.7}$$

المنارة للاستشارات
www.manaraa.com

where λ is the wavelength and n_0 is the refractive index of the background [21]. This critical power is 125.5 MW for a wavelength of 248 nm in air. If allowed to act in the absence of other effects, self-focusing can lead to a catastrophic collapse of the pulse. However, MPI and associated plasma defocusing counteract this effect to create filaments.

There are two main models that describe the phenomenon of filamentation. Extensions of these two models attempt to explain certain aspects of filamentation with greater accuracy. First, the moving focus model considers the filament as an illusion. The pulse is broken into time slices that are assumed only weakly coupled to each other. Each time slice has its own power which allows the slices with power greater than P_{cr} to be focused and those with power less than P_{cr} to diffract [12].

The second model, self-guiding, has two iterations. It begins with the self-trapping model that suggests that a strict equilibrium between diffraction and self-focusing, often called the Townes mode, is what enables filamentation to occur. This equilibrium was adjusted with the self-channeling model to loosen the strictness of the balance and include refraction from plasma generated by the intense laser pulse. This addressed the problem of instability of self-trapping that led to either an inevitable collapse of high powered pulses or an eventual diffraction of low powered pulses on the same order as normally propagated beams [12].

المنارة للاستشارات
www.manaraa.com

The dynamic spatial replenishment model is a combination of the previous two main models. This model shows that the leading edge of the pulse forms a peak due to self-focusing which generates a plasma that causes the trailing edge of the pulse to defocus and the leading peak to lessen in intensity due to MPI. As the peak intensity is lowered, the plasma is then turned off, allowing the pulse to self-focus once again until this scenario repeats itself enough to make the pulse power insufficient for refocusing [12]. This model allows for the long distance propagation of the filaments and is the foundation for this research.

The spatiotemporal soliton or light bullet is the proposed idea of a soliton forming in both space and time due to nonlinear spatial effects, such as self-focusing, that compensate for diffraction, and self-phase modulation that compensates for the spreading of the beam in time. However, this proposal is highly unlikely and has never been observed experimentally. This is probably due to the instability of the Townes modes discussed earlier and the neglect of physical effects always present in practice that would prevent a light bullet from propagating longer distances than normal diffraction and dispersion lengths [12].

X-waves or Bessel-X waves are one more suggested solution to explain filamentation. They are wave packets that propagate without undergoing natural spreading due to diffraction or dispersion. They form an X shape in both the near and far fields as represented in Figure 2.1. These peculiar waves come from

المنارة للاستشارات
www.manaraa.com

a localized stationary solution of the form

$$\mathcal{E}(r,t) = \frac{1}{2\pi}\int \mathrm{d}\omega f(\omega) J_0(\sqrt{kk''}|\omega|r) exp(-i\omega t), \tag{2.8}$$

for equation (2.4) if only the first two right hand side terms are considered. In equation (2.8) $f(\omega)$ is any narrow spectral function [12]. Because X-waves have been observed to share many characteristics of femtosecond filaments, they are a promising concept for the interpretation of filamentation.

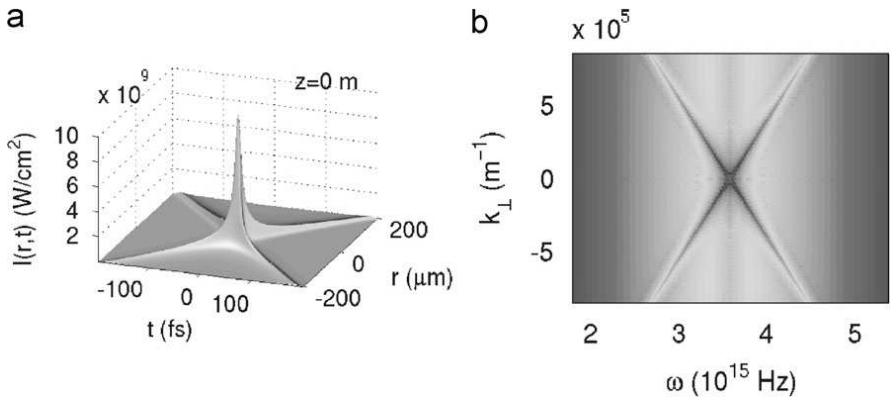

Figure 2.1: This figure shows how an X-wave has the same shape in both (a) the r-t domain or near field and (b) the k-ω domain or far field. Taken from Ref [12].

Group Velocity Dispersion

There are many different effects that can be included in an investigation of the long distance propagation of laser pulses, depending on the assumptions and approximations made. Niday [21, 23] and Schwarz and Diels [11] did not include the GVD term in their propagation equation due to the assumption that the pulses they were dealing with were long enough to ignore GVD. This assumption was

المنارة للاستشارات
www.manaraa.com

reasonable for the initial pulse durations, but with the collapse events generated in Niday's code being on the order of femto- and pico- seconds, it is important to revisit the relevance of GVD. Muller claimed that GVD did not affect pulses longer than 100 fs in duration [8], but since he could not achieve convergence of the collapses, he was not able to confirm that GVD did not effect the formation of these collapses. Although the pulses being studied here are long (on the order of picoseconds), the group velocity dispersion term must not be ignored due to the collapse events having durations on the order of tens of femtoseconds. With parts of the propagating pulse being so short, GVD should be included to accurately model the collapse event's behavior during propagation.

GVD comes from the dependence that a wave's velocity has on its frequency. This causes the different frequencies of the wave to spread out temporally as a result of the different velocities. It works in a similar way to how diffraction spreads a pulse out spatially. Extracting the GVD portion from our propagation equation (2.3) we have

$$\frac{\partial \mathcal{E}}{\partial z} = -\frac{ik''}{2}\frac{\partial^2 \mathcal{E}}{\partial t^2}. \tag{2.9}$$

With a little rearranging, this can then be compared to the one dimensional spatial propagation of a Gaussian beam as described by

$$\frac{\partial^2 \psi}{\partial y^2} - 2ik\frac{\partial \psi}{\partial z} = 0, \tag{2.10}$$

المنارة للاستشارات
www.manaraa.com

from equation (4.7.11) in reference [26]. Thus, to solve for the GVD parameter, one can use a similar process as with a 1D Gaussian beam.

In order to ensure accuracy, the value of k'' was explicitly calculated, since there are varying values in the literature. Recognizing the difference in field representations of equations (2.2) and Verdeyen's (4.7.4) with opposite signs in the exponentials, one concludes that Verdeyen's β_2 is equivalent to k'' in equation (2.9). Verdeyen goes on to define β_2 as $(\lambda^3/2\pi c^2) \cdot (d^2n/d\lambda^2)$. To determine this value, one needs the index of refraction for air in terms of wavelength. This is obtained using Cauchy's Formula [27]

$$n_{air} = 1.000287566 + \frac{1.34 \times 10^{-18}\text{m}^2}{\lambda^2} + \frac{3.777 \times 10^{-32}\text{m}^4}{\lambda^4}. \tag{2.11}$$

Using this information, a value of $k'' = 1.45$ fs^2/cm was obtained for $\lambda = 248$ nm. This value is what is used in this study and is between Couairon's value of k'' =1.21 fs^2/cm [9] and Schwarz's value of k'' =2 fs^2/cm [22]. The fact that this term is positive affirms that we are dealing with normal and not anomalous dispersion.

The reason GVD plays a part in the broadening of the duration of these collapse events is the dependence of the dispersion length, L_D, on the pulse half-width in time, t_p, of

$$L_D = \frac{t_p^2}{k''}. \tag{2.12}$$

المنارة للاستشارات
www.manaraa.com

If the pulse duration is small, this dispersion length, or distance the pulse travels before it is temporally broadened by a factor of $\sqrt{2}$, will also be small allowing GVD to broaden the pulse in the distances being propagated during these simulations. In accordance with the widths obtained for the collapse events once the collapses form, $L_D \approx 20$ cm. By including this GVD parameter in the code, it is thought that the collapsing events of the pulse may be limited by the temporal dispersion effects.

Theoretical Summary

In summary, the propagation equation used to describe the behavior of a pulse of light is based on Maxwell's equations. The terms included in this study represent transverse diffraction, multi-photon ionization, plasma generation and absorption, Kerr self-focusing, and group velocity dispersion. This last term was added to the study because of the small duration of the collapse events being investigated. The value of k'' for GVD was established as 1.45 fs^2/cm. Terms such as the Raman effect, Raleigh scattering, avalanche ionization, and plasma diffusion were neglected according to valid assumptions based on the research parameters. Long distance propagation is obtained by filamentation of the pulse when the power reaches a certain critical power to induce self-focusing. Many theoretical models have been proposed to explain this filamentation such as the dynamic spatial replenishment model which suggests somewhat of a tug-of-war

المنارة للاستشارات
www.manaraa.com

game on the intensity by self-focusing and MPI that keeps the pulse propagating. There is also the possibility that X-waves could be a description of filamentation.

المنارة للاستشارات
www.manaraa.com

III. Methodology

This chapter will describe the basic physical and numerical parameters used in the simulations of the propagation of UV pulses. A table presenting the parameters used in the bulk of the simulated runs is provided for the convenience of the reader. We will go into the details of how the code is written, to include an explanation of the split operator method and what limitations are incurred due to numerical analysis. Details of the modification of the original code of Niday's will also be discussed.

Physical and Numerical Parameters

A summary of the physical and numerical parameters used in this study will be very useful to the reader when trying to understand exactly how the results presented in this thesis were obtained. The key input parameters for the initial condition of the pulse are waist size, pulse duration, pulse power or peak intensity, and desired grid size. The default initial parameters used are specified in Table 3.1. A few of the actual grid parameters varied quite a bit from run to run such as N_t and $\triangle t$, so they are not included in this table. They will be specified appropriately when data is presented along with any parameters that are different from the values stated here.

A few notes on these values are needed to ensure clarity. The values of N_x, N_y, $\triangle x$ and $\triangle y$ were used based on the parameter study by Muller [8] for the waist size w_0. The supergaussian order, M, is used in the time dimension to

المنارة للاستشارات
www.manaraa.com

Table 3.1: Parameters for UV pulse simulations

Parameter	Variable	Value	Units
Number of grid points in x-direction	N_x	128	—
Spacing of grid points in x-direction	$\triangle x$	8	μm
Number of grid points in y-direction	N_y	128	—
Spacing of grid points in y-direction	$\triangle y$	8	μm
Wavelength	λ	248	nm
Supergaussian order	M	10	—
Pulse Duration (half-width)	t_p	5	ps
Distance of each propagation step	$\triangle z$	0.5	mm
Input power	P_{in}	250	MW
Critical power	P_{crit}	125.5	MW
Pulse waist	w_0	120	μm
Nonlinear index of refraction	n_2	7.8×10^{-23}	m^2/W
Linear loss	α_L	2.5×10^{-4}	m^{-1}
MPI order	K	3	—
MPI coefficient	$\beta^{(K)}$	3.9×10^{-34}	m^3/W^2
Inverse Bremsstrahlung cross section	σ	5.2×10^{-25}	m^2
Electron collision time	τ	0.35×10^{-13}	ps
Old radiative recombination rate	α	1.1×10^{-12}	m^3/s
New radiative recombination rate	α_n	1.3×10^{-14}	m^3/s
GVD Parameter	k''	1.45154×10^{-28}	s^2/m

المنارة للاستشارات
www.manaraa.com

simulate the beginning, middle, and end of an actual pulse with duration t_p as defined by a one dimensional Gaussian of

$$E(t) = E_0 e^{-\left(\frac{t}{t_p}\right)^{2M}}. \tag{3.1}$$

This is in order to simulate a steady state for much of the duration of the pulse. However, the beginning and the end of the pulse will not satisfy the steady state solution. The old radiative recombination rate in the table was initially used based on many references [5,8,13,21,23]. This value was supposedly an improvement on a value used by Schwarz of 5×10^{-13} m^3/s [22]. Recently, though, Chalus presented a newer value for α which is defined in the table as the 'new' radiative recombination rate α_n. Many of the simulations done in this research were performed with this updated value and will be specified when appropriate.

Numerical Methods

All simulations done for this research used FORTRAN code derived from what was originally written by Niday [21]. His three dimensional code uses a three dimensional grid or array to hold the information representing the field. Symmetry in the x and y directions is assumed for the initial condition of the Gaussian pulse. Time is the third dimension of the array and can be related to the third spatial dimension by $z = c\triangle t$ where c is the speed of light, $\triangle t$ is the amount of time that has passed, and z is the direction of beam propagation. At each propagation or

المنارة للاستشارات
www.manaraa.com

z- step, the pulse is represented with an x, y, and t array where $t = 0$ is located at z. The reference frame moves at a speed equivalent to the group velocity of the pulse in order to record the pulse's evolution at each distance z. If the reference frame was fixed, the pulse would go off the time grid almost immediately after beginning to propagate because the speed of light is so much larger than the size scale of the pulse and grid. By allowing the reference frame to move with the pulse, we are able to use grid sizes and spacings that can accurately describe the pulse as it propagates. As the grid spacing decreases, the grid size (number of points on the grid) must increase to account for the same sized pulse. This, in turn, dramatically increases the amount of time and memory space needed to compute the information. Thus, there is a delicate balance between resolution and practicality. Figures 3.1 through 3.3 are an example of the 3D plots that can be generated by the GUI interface associated with Niday's code. These figures show the evolution of a pulse with a time history plot of the field with respect to the x axis along with its fluence profile at various propagation distances. It is a ten picosecond pulse generated with the new recombination rate and no GVD, represented on a grid with $N_t = 4096$ and $\triangle t = 3$ fs. Note that at 50 cm the fluence profile begins to look square. This means it is no longer an accurate representation since the fluence has gone off the spatial grid and has begun to be confined by the grid, the absorbing boundary conditions reflecting nonzero values.

المنارة للاستشارات
www.manaraa.com

In Niday's 3D propagation code, the x, y, and t dimensions are transformed via a Fast Fourier Transform (FFT) as required by the split operator method which is explained in the following paragraph. In order for the FFT to work efficiently, the number of grid points in each dimension need to be chosen as powers of two. Originally, Niday's code contained two 3D arrays to represent the field: one array for the x, y, and t dimensions in real space and the other array for the k_x, k_y, and Ω dimensions in frequency or k- space after the Fourier transform. Having a copy of the field in both the space/time and frequency domains allowed for more freedom in the manipulation of the field within the code. However, as resolution needed to be increased, the size of the grid also had to be increased. With the original code, when the grid size was doubled, the memory needed to hold both of the field arrays quadrupled. By eliminating the extra array dedicated to the k-space representation of the field, the grid size was able to double once more beyond what was previously allowed. To do this, the code was adjusted to keep only one array in memory for the field. This array, therefore, switched between real and k-space. With the ability to have a larger grid size, the resolution in the time domain was able to be increased. This helped to converge the collapse events in the time domain.

The split operator method is used by Niday in his code to solve the pulse propagation equation (2.4), which can be simplified to

$$\frac{\partial \mathcal{E}}{\partial z} = i\hat{T}\mathcal{E} + i\hat{V}\mathcal{E}, \tag{3.2}$$

المنارة للاستشارات
www.manaraa.com

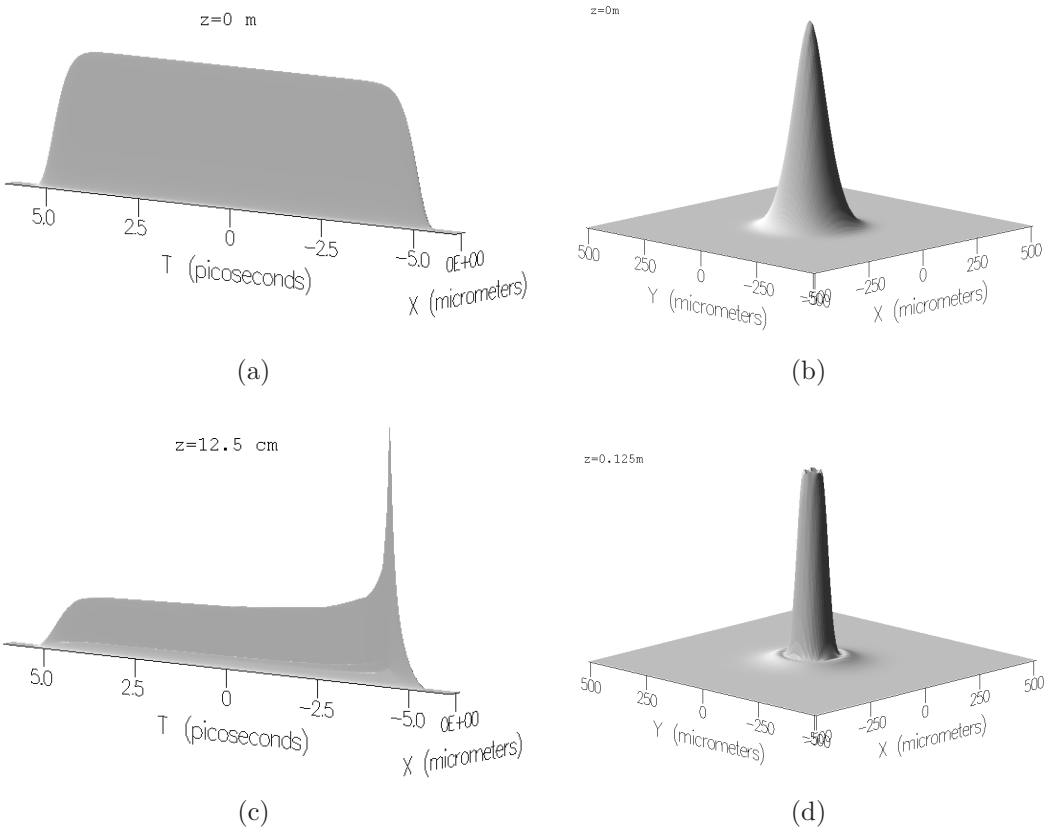

Figure 3.1: Left Column: Full 3D view of pulse propagation with its leading edge to the right in the negative time domain. Right Column: Corresponding fluence profiles at propagation distances of 0 and 12.5 cm.

المنارة للاستشارات
www.manaraa.com

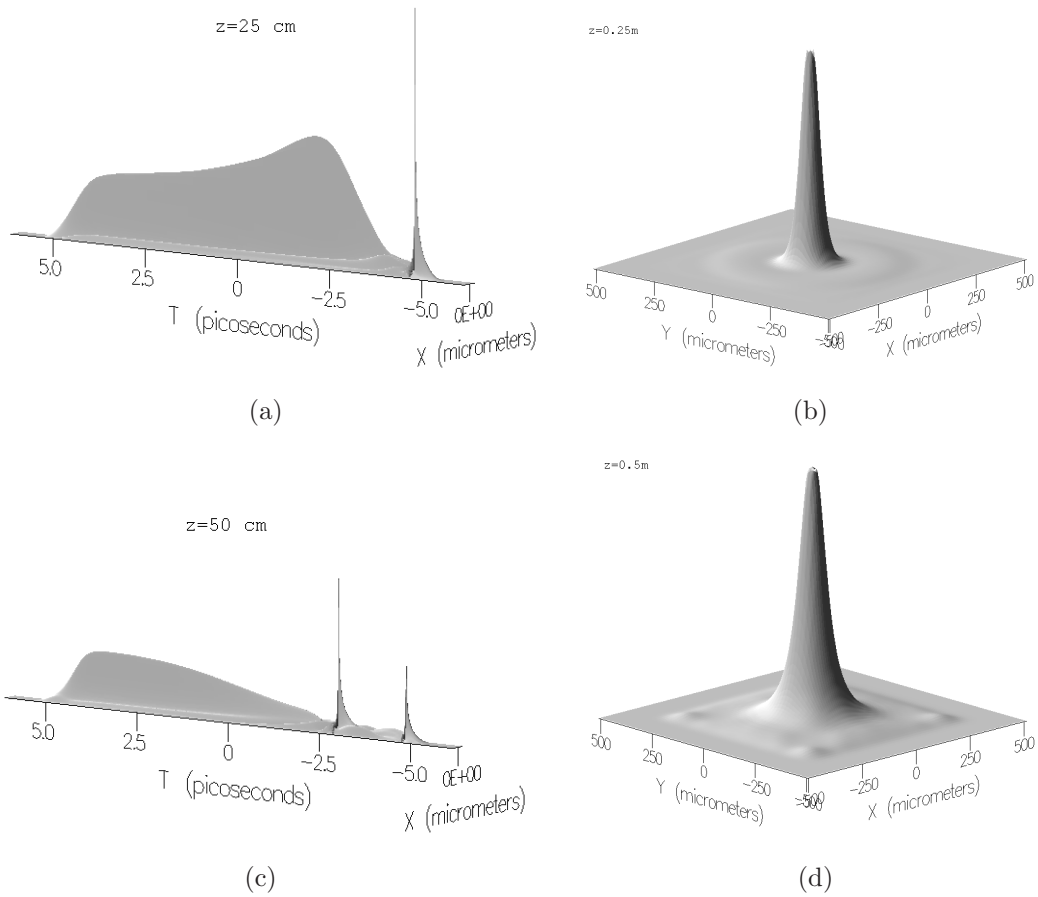

Figure 3.2: Left Column: Full 3D view of pulse propagation with its leading edge to the right in the negative time domain. Right Column: Corresponding fluence profiles at propagation distances of 25 cm and 50 cm. Note the evidence in the fluence profile of going off the spatial grid.

المنارة للاستشارات
www.manaraa.com

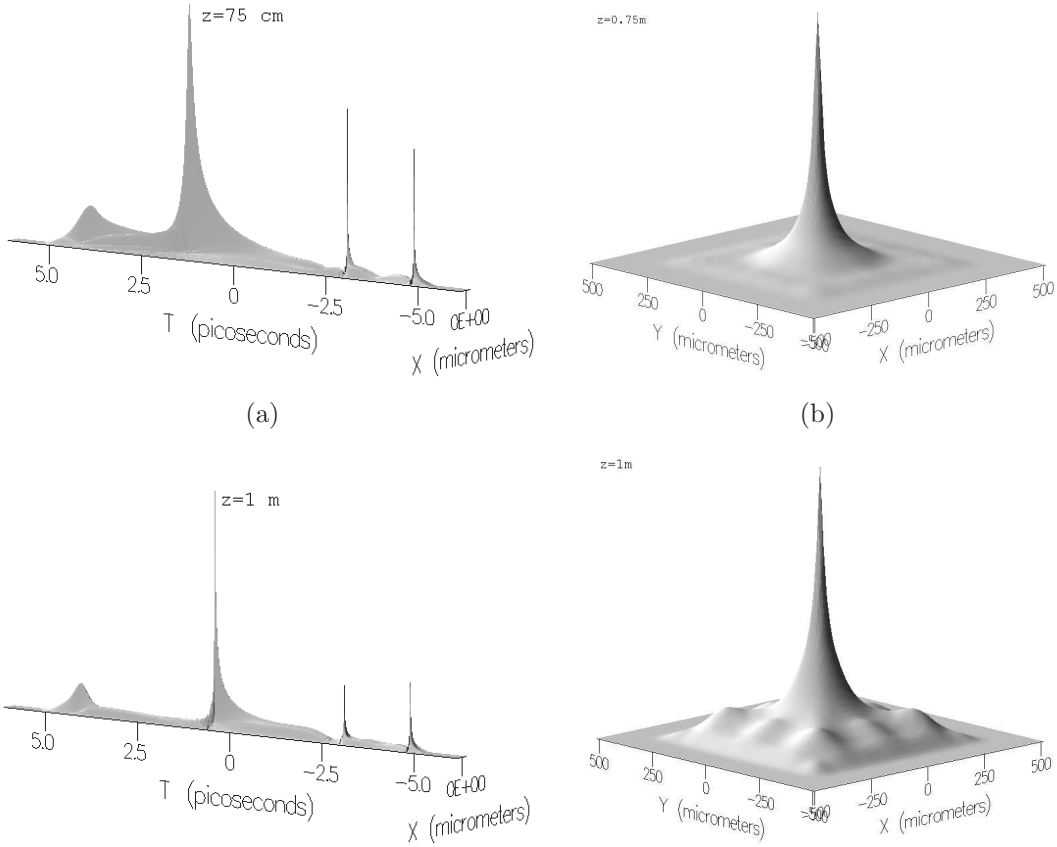

(a) (b)

(c) (d)

Figure 3.3: Left Column: Full 3D view of pulse propagation with its leading edge to the right in the negative time domain. Right Column: Corresponding fluence profiles at propagation distances of 75 cm and 1 m. Figure 3.4 shows that the pulse has not gone off the k and Ω grids by these propagation distances.

المنارة للاستشارات
www.manaraa.com

where we have

$$i\hat{V} = ik_0 n_2 |\mathcal{E}|^2 - \frac{\beta^{(K)}}{2}|\mathcal{E}|^{2K-2} - \frac{\sigma}{2}\left(1 + i\omega\tau\right)\rho \quad \text{and} \tag{3.3}$$

$$i\hat{T} = i\frac{1}{2k_0}\nabla_\perp^2 - \frac{ik''}{2}\frac{\partial^2}{\partial t^2}\ . \tag{3.4}$$

Equation (3.3) is the nonlinear index change piece and will be diagonal in the spatial representation for $\mathcal{E}$. Equation (3.4) is the linear diffraction and GVD piece and is diagonal in the spectral representation of $\mathcal{E}$ or in k-space. The split operator method represents the incremental step propagator $e^{i\hat{H}\triangle z}$ as

$$e^{i\frac{\hat{T}\triangle z}{2}} e^{i\hat{V}\triangle z} e^{i\frac{\hat{T}\triangle z}{2}} + \mathcal{O}(\triangle z^3), \tag{3.5}$$

where $i\hat{H} = i\hat{T} + i\hat{V}$. In order to use this method effectively to solve for the solution $\mathcal{E}(z + \triangle z) = e^{i\hat{H}\triangle z}\mathcal{E}(z)$, we apply the three separate exponential parts of equation (3.5) at different times while transforming $\mathcal{E}$ between its real and spectral representations. First, the FFT is taken, putting $\mathcal{E}$ into k-space, then the first half of the $\hat{T}$ operator is applied in its spectral representation according to

$$e^{i\frac{\hat{T}\triangle z}{2}}\mathcal{E}(k_x, k_y) = e^{-i\left(\frac{k_\perp^2}{4k_0} + \frac{k''\Omega^2}{4}\right)\triangle z}\mathcal{E}(k_x, k_y). \tag{3.6}$$

This spectral representation of the $\hat{T}$ operator can be determined for each point on the k grid, that is, each value of $k_\perp$ and Ω at the beginning of the code

المنارة للاستشارات
www.manaraa.com

after the first FFT. It does not have to be recomputed for each propagation step. Transforming equation (3.6) back into its spatial representation with an inverse FFT, the nonlinear index change piece is then applied by multiplying by $e^{i\hat{V}\triangle z}$. Another Fourier transform puts $\mathcal{E}$ back into spectral space to allow for the second half of the $\hat{T}$ operator to be applied in the same way as the first half.

Limitations of Numerical Methods

Using this split operator method creates a requirement for the grid size and spacing to ensure accuracy. Both the spatial and spectral grids must contain adequate resolution and extent to represent the full field. For this split operator approximation to work well, the values in the exponentials should be small so that the arguments of the exponential phase factors will be smaller than unity. Including the GVD term, we have for the maximum absolute value of $\hat{T}$,

$$|\hat{T}|_{max} = |\frac{k_\perp^2}{2k_0} - \frac{k''\Omega^2}{2}|_{max} \ . \tag{3.7}$$

The value on the right hand side is maximized when the bigger of the $k_\perp$ and Ω terms is at its max and the smaller is zero since both terms are always positive. For $\triangle x$ =8 μm, $\triangle t$ has to be less than 0.5 fs to allow the Ω term to dominate. Since the smallest $\triangle t$ we use is 0.9 fs, we set Ω^2 equal to zero and have just the

المنارة للاستشارات
www.manaraa.com

$k_\perp$ term with which to deal. This gives a maximum exponential argument of

$$\frac{|\hat{T}|_{max}\triangle z}{2} = \frac{\pi^2 \triangle z}{4k_0 \triangle x^2} \ . \tag{3.8}$$

Setting this to be less than unity and solving for $\triangle z$ gives

$$\triangle z \leq \frac{4k_0 \triangle x^2}{\pi^2}, \tag{3.9}$$

which is the same condition that Niday found [21]. With an UV wavelength of 248 nm and $\triangle x$ =8 μm, $\triangle z \leq 0.67$ mm. This condition is satisfied with our choice of $\triangle z = 0.5$ mm (see Table 3.1). If $\triangle t$ is small enough to allow the Ω term to dominate in equation (3.7), $\triangle z$ would then be limited by

$$\triangle z \leq \frac{4\triangle t^2}{k'' \pi^2}. \tag{3.10}$$

The biggest limitations of numerically solving the propagation equations to describe UV filamentation are computing power and time. A computer with two dual processors totaling 16 GB of RAM has been used for the computations presented here. The longest, most detailed runs took up to six days to complete. The smaller runs (propagating less distance and with less resolution) took 12 to 36 hours, thus limiting how many runs were able to be performed and the resolution able to be achieved in the time frame given for this research. The code

المنارة للاستشارات
www.manaraa.com

was modified to use almost 50% less memory in order to be able to achieve a time step of 0.9 fs that was needed to show convergence. Since this run took over 12 GB of the 16 total available and the FFT requires the dimensions of the grid to be in powers of 2, increasing the grid size to accommodate a smaller change in time would require almost a doubling of the memory needed for computation, putting it well above the computer's limit.

Another facet of numerical limitation involves the k-space representation of the pulse. In Muller's research, he found that after a certain distance of propagation, the trailing edge of the pulse would start to exhibit collapse. This was thought to be due to numerical parameters chosen that allowed the field to overflow the Ω-grid, causing the values to wrap around the grid. This research, however, does not see this manifestation of the grid overflow. Figure 3.4 shows the k representation of the pulse in Figures 3.1 through 3.3 at propagation distances of 2.5 cm, 12.5 cm, 50 cm, and 1 m. Notice how the pulse does not go off the k- or Ω-grid, thus, in Figures 3.2 and 3.3 the pulse does not produce collapses on its trailing edge. Also notice how the fluence profile begins to show the squareness of the grid rather than being spherical at only 50 cm. This means that the pulse has diverged to the extent of going off the spatial grid. The results of the propagation code after this point are no longer accurate due to the grid's artificial limitations.

المنارة للاستشارات
www.manaraa.com

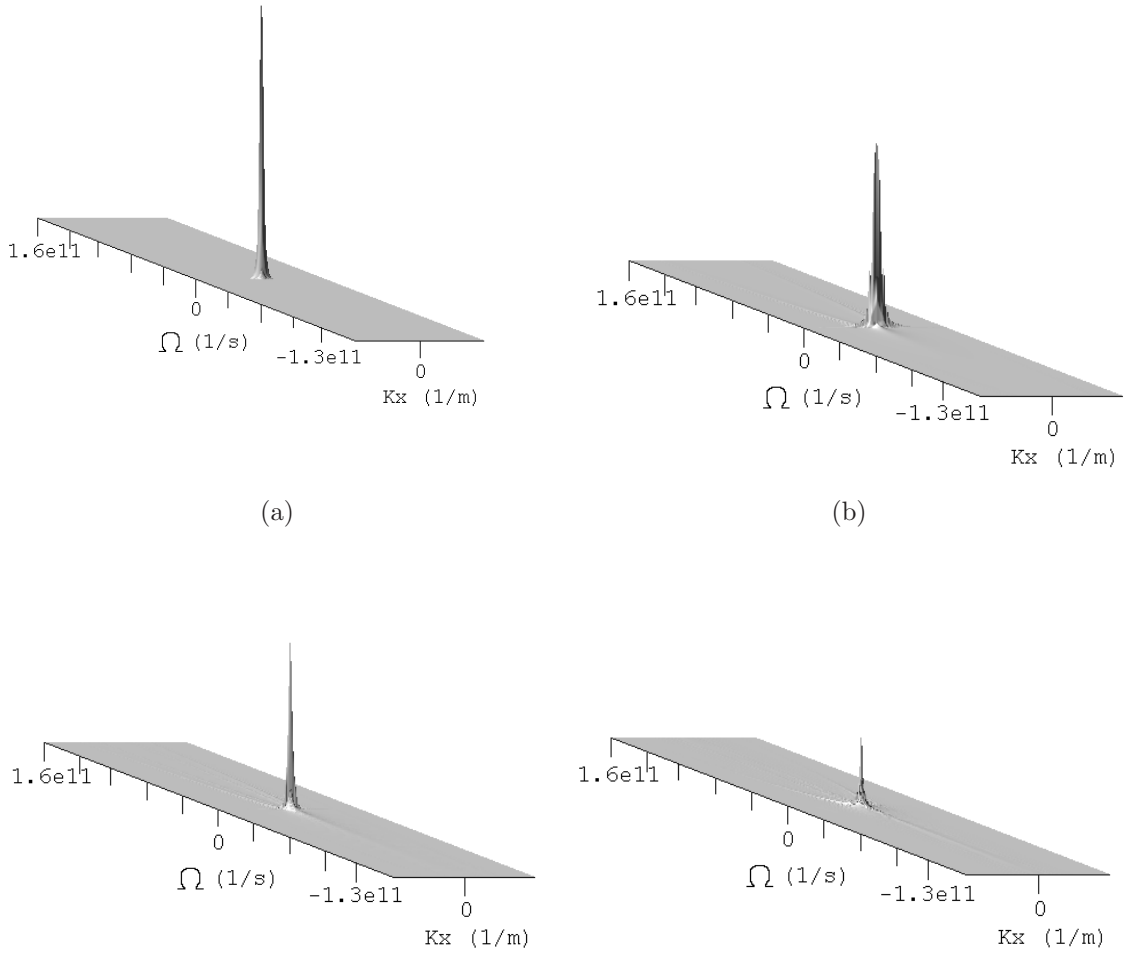

Figure 3.4: Frequency representation of the propagating pulse from Figures 3.1 through 3.3 at 2.5 cm, 12.5 cm, 50 cm, and 1 m. Note that the pulse has not gone off the k_x or Ω grid. All plots are on the same scale.

المنارة للاستشارات
www.manaraa.com

To help prevent this wrap around effect in the space dimensions, absorbing boundary conditions (ABC's) are used in the code according to

$$
\begin{aligned}
abc = &- \frac{\mathrm{S}\triangle z}{4} \exp\left(-\frac{(f(x,y) - f(x_{min},y))^2}{\mathrm{W}}\right) \\
&- \frac{\mathrm{S}\triangle z}{4} \exp\left(-\frac{(f(x,y) - f(x_{max},y))^2}{\mathrm{W}}\right) \\
&- \frac{\mathrm{S}\triangle z}{4} \exp\left(-\frac{(f(x,y) - f(x,y_{min}))^2}{\mathrm{W}}\right) \\
&- \frac{\mathrm{S}\triangle z}{4} \exp\left(-\frac{(f(x,y) - f(x,y_{max}))^2}{\mathrm{W}}\right),
\end{aligned}
\tag{3.11}
$$

where S is the strength of the ABC's of 5000 and W is a width of 0.5×10^{-8}. The field is multiplied by e^{abc} during the middle step of the split operator method while in real space. This subdues the values of the field at the edges of the spatial grid, preventing them from being wrapped around to the other side of the grid, while making sure not to eliminate values big enough to make a difference in the pulse profile. ABC's were not, however, applied in the time dimension for fear that important information relevant to the propagation of the pulse would be ignored. This required the time grid to maintain a large buffer between the edge of the pulse and the edge of the grid to allow for dispersion.

Summary of Methodology

In summary, the code written by Niday in FORTRAN to describe the propagation of a pulse through air uses the split operator method to apply a linear operator to the field in real space and a nonlinear operator in k-space by using a

المنارة للاستشارات
www.manaraa.com

FFT to convert the field. ABC's were applied to prevent diffracting field values at the edge of the spatial grid from wrapping around and causing nonphysical effects in the propagation code. Using the split operator method creates a requirement for the grid parameters, which, in this case, restricts the z-step to an upper limit of 6.7 mm. The numerical parameters are also limited by computational power and efficiency. The code was modified to use less memory in order to increase the grid size to $N_t = 16384$ and decrease the grid spacing to $\triangle t = 0.9$ fs in the time domain to achieve maximum resolution with the equipment available. The values of most of the parameters are specified in Table 3.1.

المنارة للاستشارات
www.manaraa.com

IV. Results and Analysis

This chapter includes the important results obtained from the research and simulations dealing with the long distance propagation of UV light. It shows that time convergence was achieved with certain parameters and explains why convergence could not be achieved at propagation distances farther than specified. It discusses the details of the collapse events obtained from the convergence runs as well as the interaction between the different terms of the propagation equation, explaining at what points certain terms dominate and act to increase or decrease this collapse phenomenon. A stability analysis is done with the inclusion of GVD, the new recombination coefficient, and the higher MPI parameter. Thought was given to the effects of the loss terms as well. In all cases, the analysis shows the inherent instability of the pulses being considered. Suggestions are given to create a more stable propagation. The results of a simulation, using the same initial conditions as an experiment producing UV filamentation, are also presented.

Time Convergence

In order to understand more about these collapse events on the leading edge of the pulse, time convergence must be achieved with the numerical parameters to make sure that the information being produced is accurately displaying what is physically happening. Using a pulse of 100 ps total duration ($t_p = 50$ ps), time convergence was achieved with an increased MPI coefficient, $\beta^{(K)} = 3.9 \times 10^{-33}$ m^3/W^2, and no GVD with a $\triangle t$ of 20 fs. Figure 4.1 shows this convergence at a

المنارة للاستشارات
www.manaraa.com

propagation distance of 1 m. The reason higher MPI leads to better convergence of the collapses is that it increases the losses enabling them to better counteract self-focusing. With self-focusing abated more quickly, the collapses do not have an opportunity to increase to such a great extent in intensity or become so short in duration, thus allowing easier representation with only a sampling of the data. With the original value of the MPI coefficient, the intensities of the collapse events are over an order of magnitude larger than what is shown here. This method of increasing $\beta^{(K)}$ was the only way Muller could achieve convergence. In this effort, convergence was also achieved without the artificially increased parameter by shortening the pulse to 10 ps, so that the numerical parameters could be tightened while the computer's processing capabilities could still manage the data.

In Figure 4.2, a pulse consisting of the old radiative recombination rate of 1.1×10^{-12} m^3/s, $N_t = 8192$, and $\triangle t = 1.35$ fs, in addition to the parameters in Table 3.1 shows convergence at a propagation distance of 20 cm as it is represented in exactly the same fashion as the same pulse with even tighter numerical parameters of $N_t = 16,384$ and $\triangle t$=0.9 fs. However, going beyond this propagation distance, the GVD causes the pulse to break down, which will be discussed in a later section. To check the convergence at farther propagation distances, runs were made with no GVD included. As the propagation distance increased, the collapse events continue to decrease in duration causing convergence to become more difficult. Figure 4.3 shows successful convergence at $z = 25$ cm and slightly

المنارة للاستشارات
www.manaraa.com

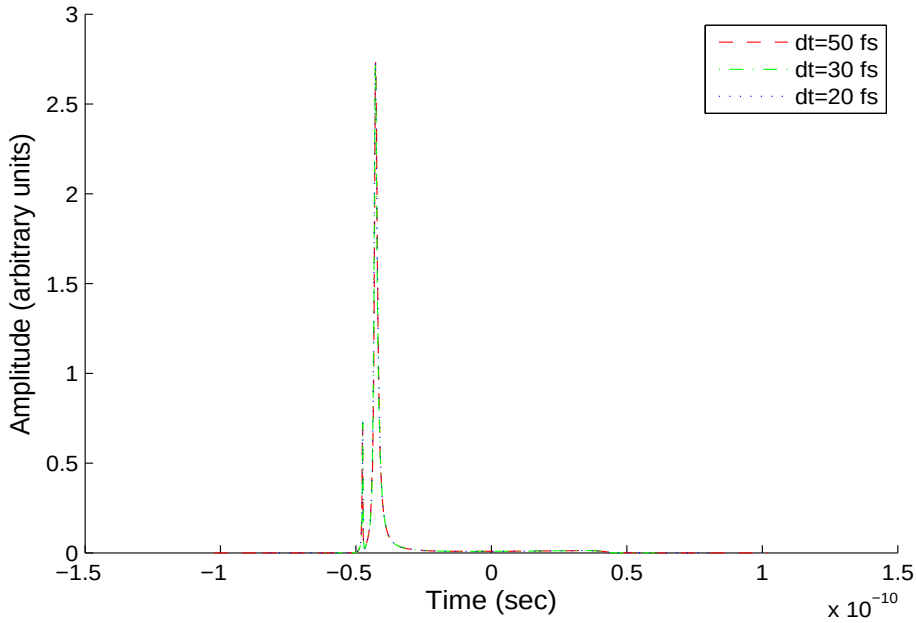

(a)

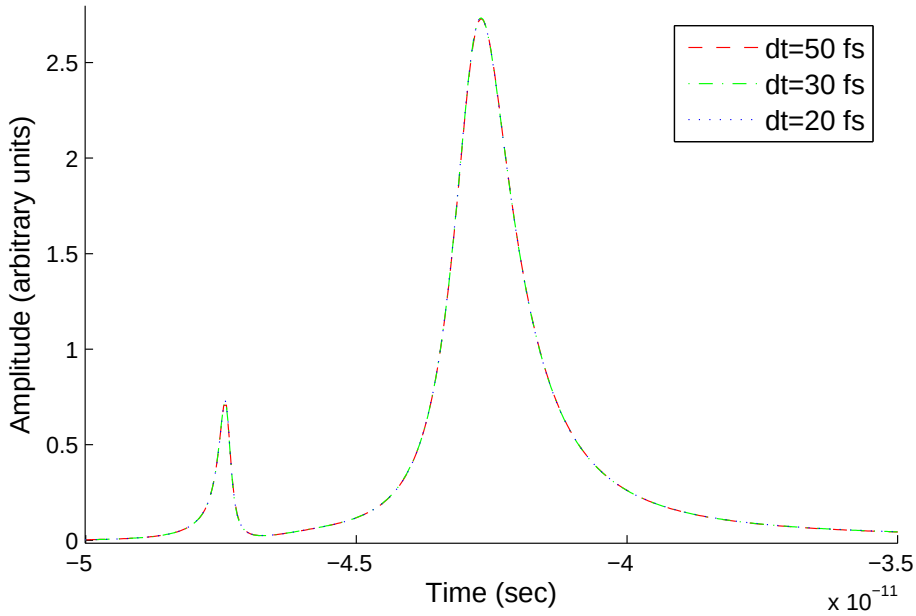

(b)

Figure 4.1: This time slice at $x = 0$ and $y = 0$ shows time convergence of a 100 ps pulse at $z = 1$ m. The initial peak amplitude is normalized to 1. Plot (b) is a magnification of the collapses in plot (a). Note that there are actually three different lines on the graph, but convergence makes them indistinguishable.

المنارة للاستشارات
www.manaraa.com

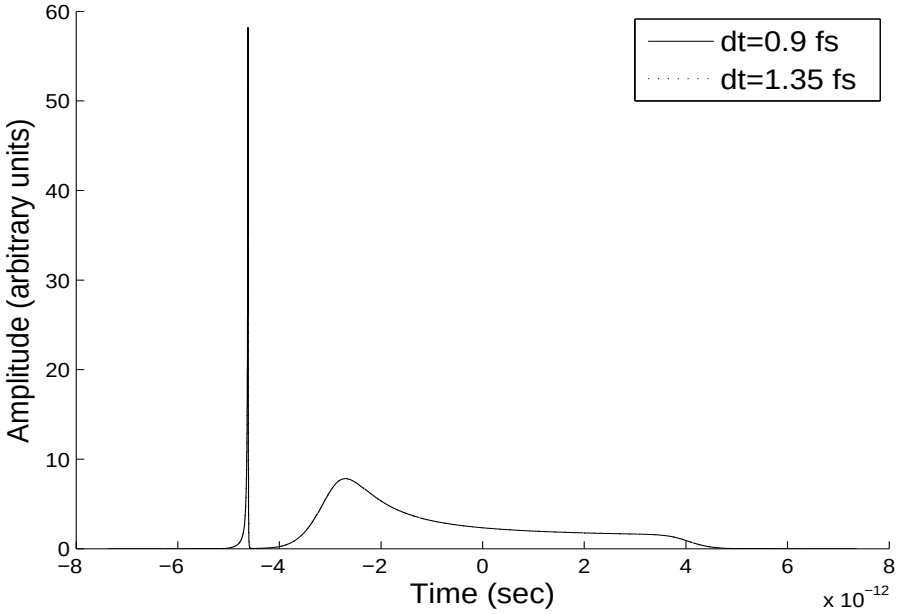

(a)

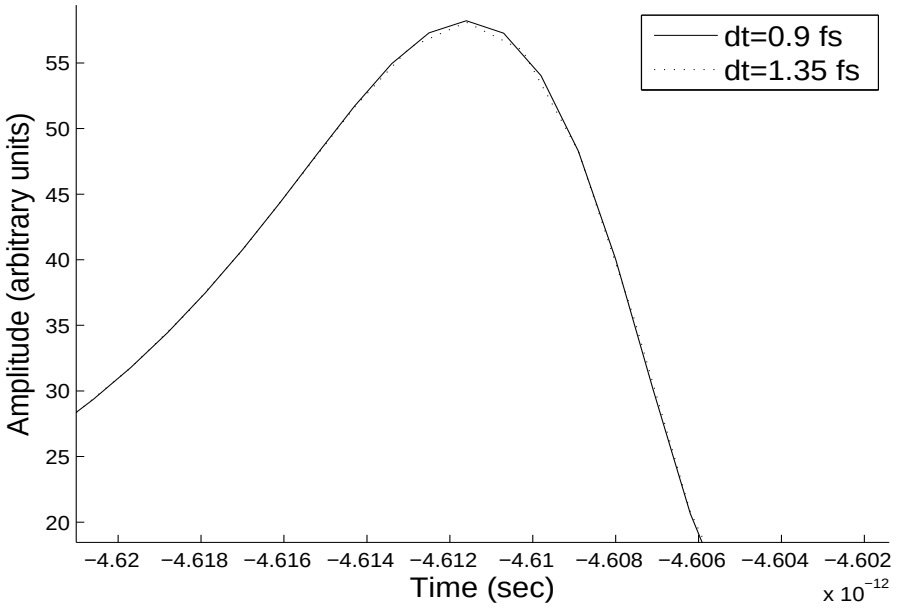

(b)

Figure 4.2: This plot shows time convergence of the pulse collapse at $z = 20$ cm. Plot (b) is a magnified portion of the collapse in plot (a). Note that the two lines are barely distinguishable due to convergence.

المنارة للاستشارات
www.manaraa.com

less successful convergence at $z = 50$ cm. It is interesting to note that the first collapse event is always accurately displayed in duration, even if the sampling frequency does not allow accurate display of the peak intensity of the collapse. The following collapses are shown to occur slightly later as $\triangle t$ is decreased. This is believed to be caused by the amount of power in the first collapse calculated by the numerical simulation. As $\triangle t$ decreases, the volume under the first collapse is more accurately assessed as being larger. With the rest of the pulse having less power with which to work, a longer time is required for a new collapse event to form, thus explaining the discrepancy in the placement of the following collapses.

Time convergence was also displayed with the new recombination rate, α_n and no GVD. See Figure 4.4. A comparison was done between the old and new recombination rates to see how this value affected the pulse formation. As shown in Figure 4.5, the value of α did not affect the formation of the first collapse at all. However, the new smaller rate required more time before the formation of the second collapse could occur. This is intuitive when one considers equation (2.6). A higher α means slower change in the plasma density. Therefore, it takes longer for the plasma to decrease enough for self-focusing to begin forming the next collapse. A plot of the plasma densities comparing both α values at $z = 12.5$ cm and $z = 25$ cm is shown in Figures 4.6 and 4.7 along with the pulse profiles at the same distances.

المنارة للاستشارات
www.manaraa.com

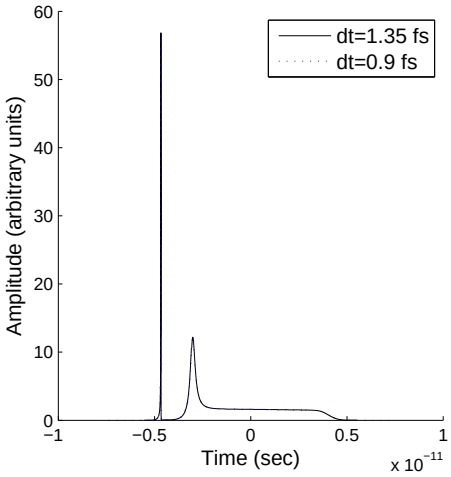

(a) $z = 25$ cm

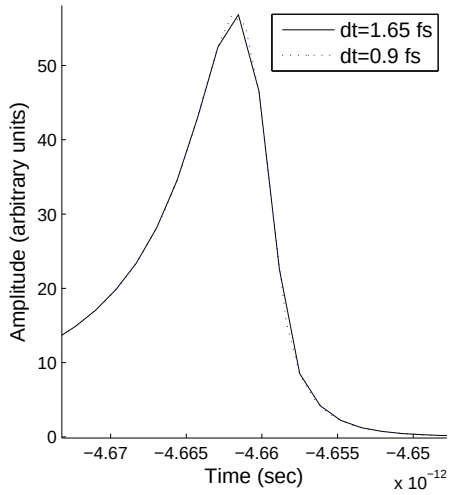

(b) First Collapse

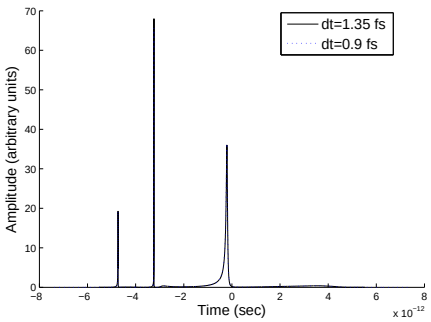

(c) $z = 50$ cm

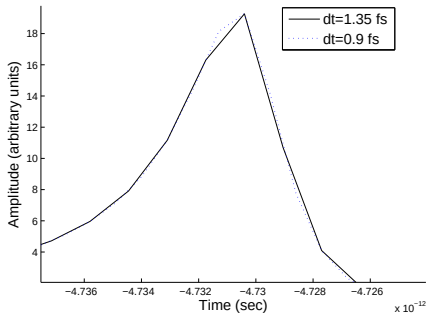

(d) First Collapse

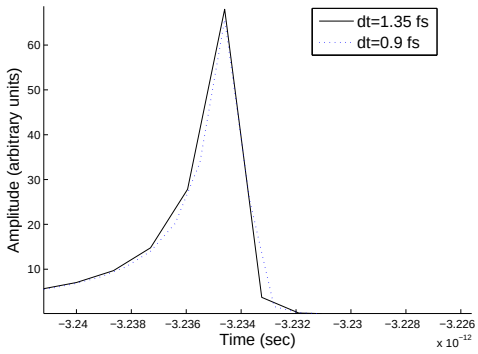

(e) Second Collapse

Figure 4.3: This plot shows time convergence of the pulse collapse without GVD and a recombination rate of $\alpha = 1.1 \times 10^{-12}$ m^3/s at $z = 0.25$ m (a,b) and $z = 50$ cm (c,d,e). Notice that at 50 cm, the peak of the first collapse (d) is being cut off due to sampling frequency, thus making the second collapse (e) slightly different than the smaller time step collapse.

المنارة للاستشارات
www.manaraa.com

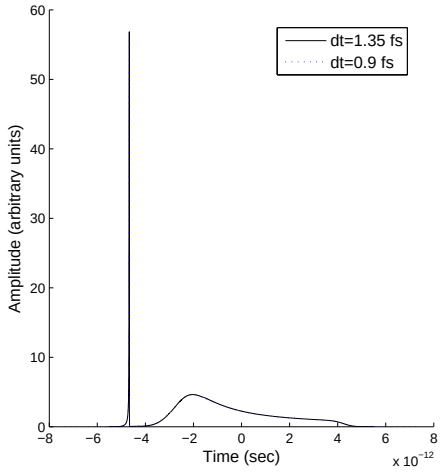

(a) $z = 25$ cm

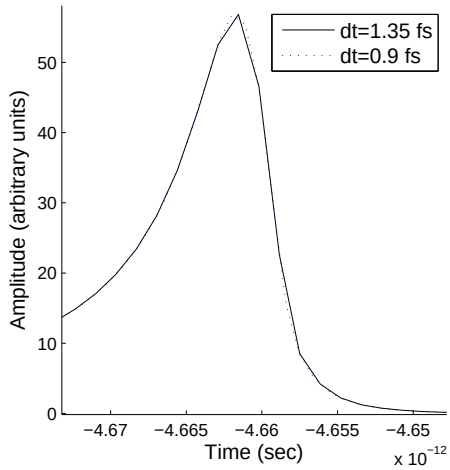

(b) First Collapse

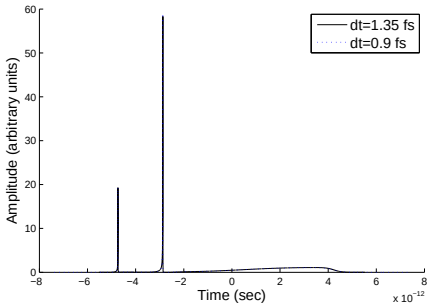

(c) $z = 50$ cm

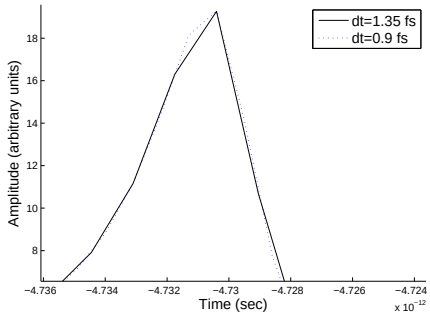

(d) First Collapse

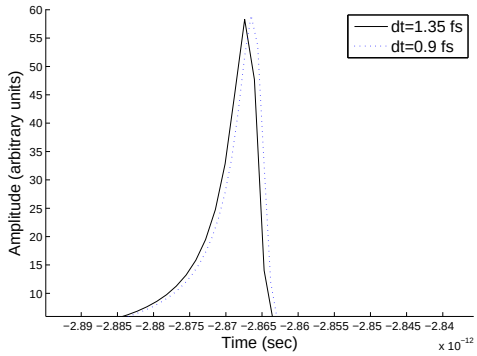

(e) Second Collapse

Figure 4.4: This plot shows time convergence of the pulse collapse without GVD and a recombination rate of $\alpha_n = 1.3 \times 10^{-14}$ m^3/s at $z = 0.25$ m (a,b) and $z = 50$ cm (c,d,e). Notice that at 50 cm, the peak of the first collapse (d) is being cut off due to sampling frequency, thus making the second collapse (e) slightly less converged.

المنارة للاستشارات
www.manaraa.com

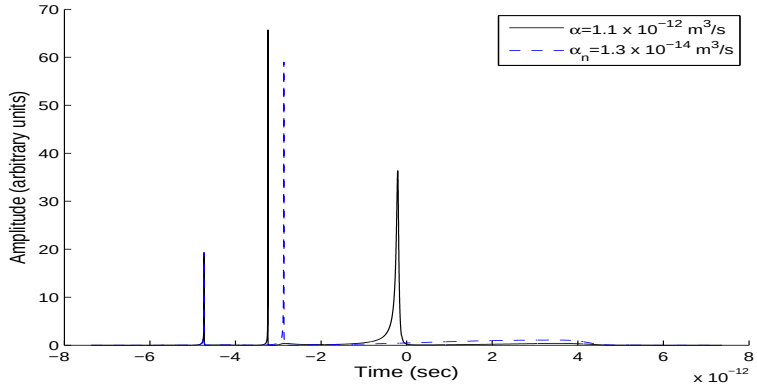

(a) Entire Pulse

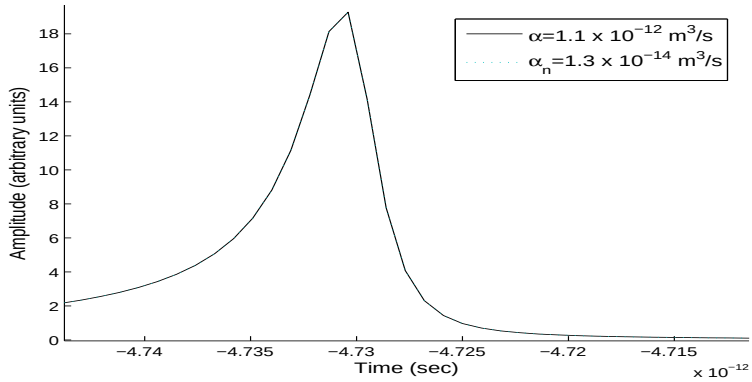

(b) First collapse

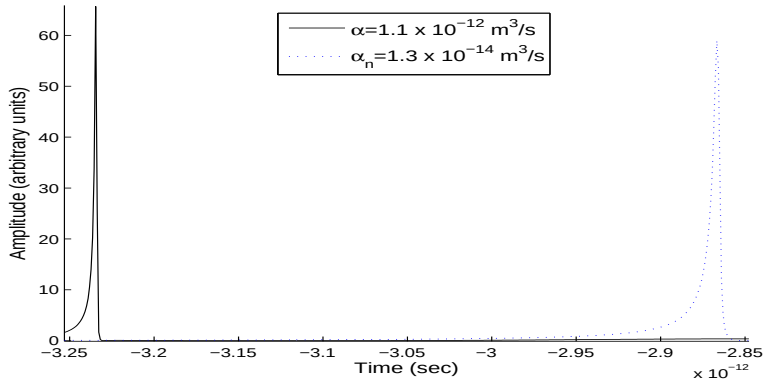

(c) Second Collapse

Figure 4.5: A pulse with both the old (solid) and new (dotted) recombination rates is shown at $z = 50$ cm with $\triangle t = 0.9$ fs and without GVD. (b) Both rates form exactly the same first collapse. (c) The second collapse forms much later with the new recombination rate.

المنارة للاستشارات
www.manaraa.com

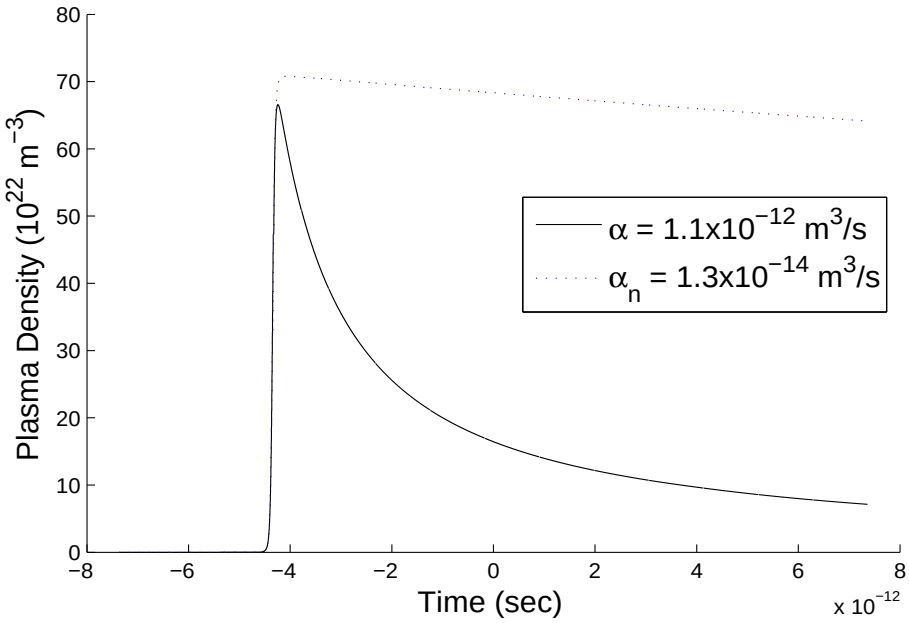

(a) Plasma

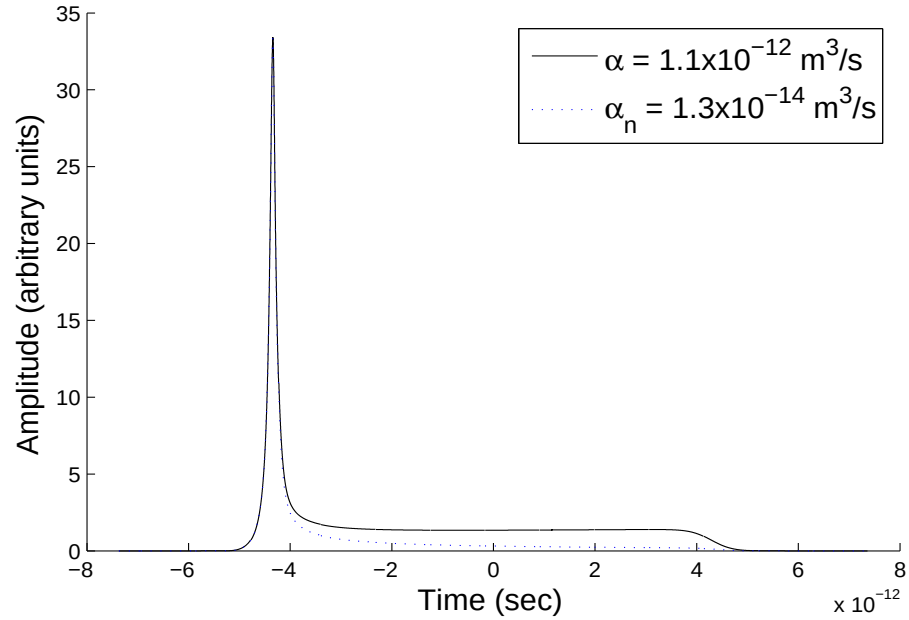

(b) Entire Pulse

Figure 4.6: (a) Illustrates how the plasma density with α_n (dotted line) decreases at a much slower rate than the plasma density with α (solid line). Shown for $z = 12.5$ cm and no GVD. (b) Corresponding pulse at $z = 12.5$ cm.

المنارة للاستشارات
www.manaraa.com

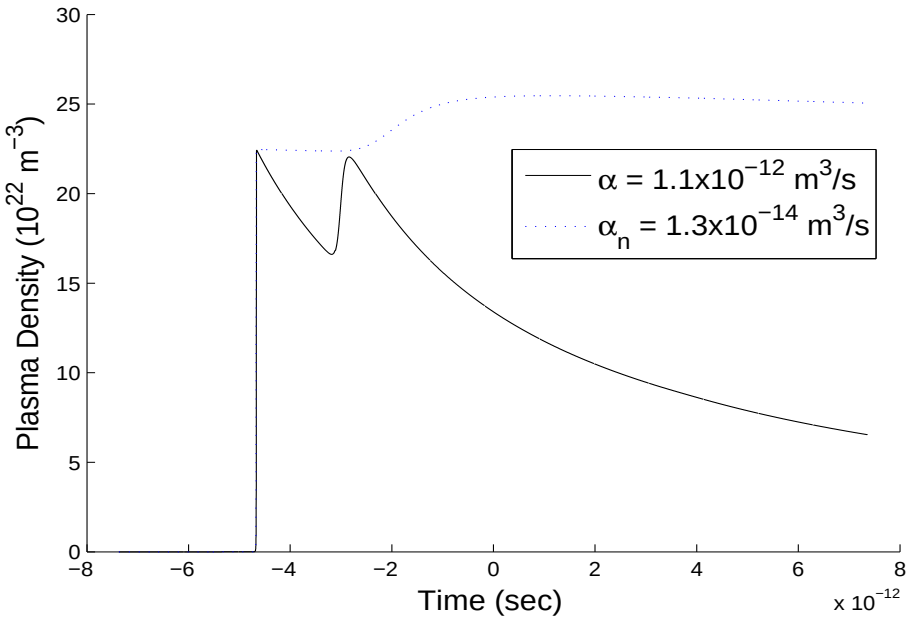

(a) Plasma

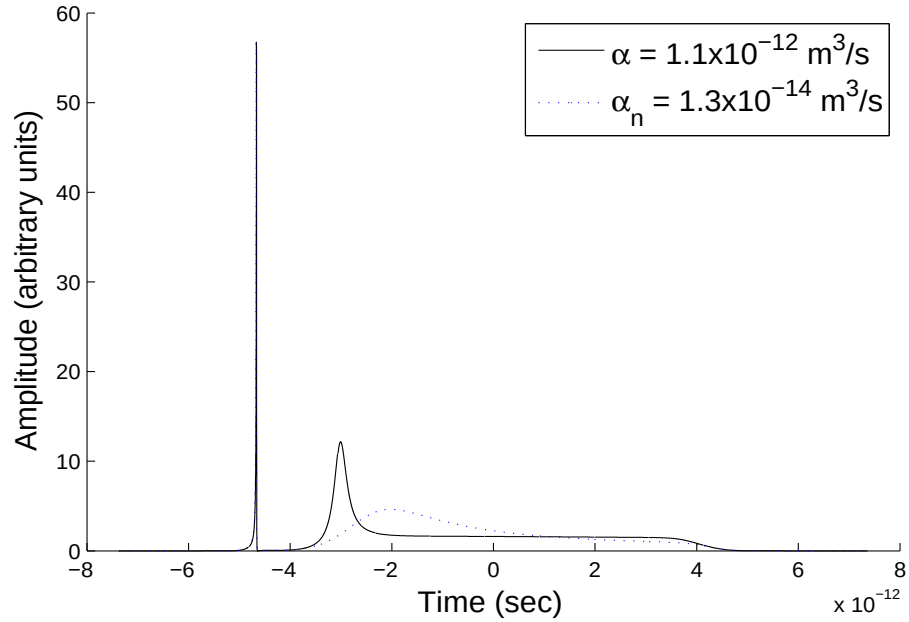

(b) Entire Pulse

Figure 4.7: (a) Illustrates how the plasma density with α_n (dotted line) decreases at a much slower rate than the plasma density with α (solid line). Shown for $z = 25$ cm and no GVD. (b) Corresponding pulse at $z = 25$ cm.

المنارة للاستشارات
www.manaraa.com

As the collapses continue to propagate, they become increasingly intense and narrow. This made it difficult to assess the behavior of these collapses at farther propagation distances. However, being able to show convergence even up to a certain propagation distance is a step in the right direction toward understanding the behavior of these collapses.

Details of Collapse Events

With time convergence of the collapse events, it was thought that the size, shape, and behavior of these occurrences could be studied. However, convergence was only achieved up to a certain propagation distance. This distance did not allow for detailed analysis of a collapse's complete evolution. Although it is clear that the collapses continue to collapse down in duration, it is not clear if this collapse continues indefinitely or stabilizes at a certain duration, since sampling frequency could not accurately describe the shape and size after a certain distance. Further research is needed to understand these collapses in more detail. An adaptive grid that can have more resolution where the collapse events are occurring and less where the pulse is somewhat stable could allow for this type of analysis. The FFT approach would have to be abandoned in the time dimension, however, requiring an entirely different method of solving the propagation equation if GVD is included. This was beyond the scope of this research.

المنارة للاستشارات
www.manaraa.com

Stability Analysis

In [21, 23], Niday performed an analysis on the stability of long UV pulses where an instantaneous index of refraction is assumed. He studied the growth of unstable modes with respect to both spatial and temporal frequencies, which will be referred to as $k_\perp$ and Ω, respectively. He found that the frequency response to the instability is unbounded, meaning that all frequencies present in the numerical model will experience growth, and this growth will not be bandwidth limited as desired for a spectral code. Thus, he concluded that long pulses suffer from modulational instability.

Following his analysis, we will discuss the stability of picosecond pulses including GVD with losses considered as well. We start with the propagation and plasma equations (2.4) and (2.6), including only the imaginary terms (i.e. no loss terms) and a simplified plasma equation, giving

$$\frac{\partial \mathcal{E}}{\partial z} = i\frac{1}{2k}\nabla_\perp^2 \mathcal{E} - i\frac{k''}{2}\frac{\partial^2 \mathcal{E}}{\partial t^2} - i\frac{\sigma\omega\tau}{2}\rho\mathcal{E} + ik_0 n_2|\mathcal{E}|^2\mathcal{E} \tag{4.1}$$

$$\frac{\partial \rho}{\partial t} = b|\mathcal{E}|^{2K} - \alpha\rho^2, \tag{4.2}$$

where $b \equiv \frac{\beta^{(K)}}{K\hbar\omega}$. We then assume a steady state solution for the field and plasma. If losses were included at this point, there would not be a steady state solution because the pulse would continuously decrease due to the losses. The steady state solutions are solved for by Niday, who shows that the exact solution for the field

المنارة للاستشارات
www.manaraa.com

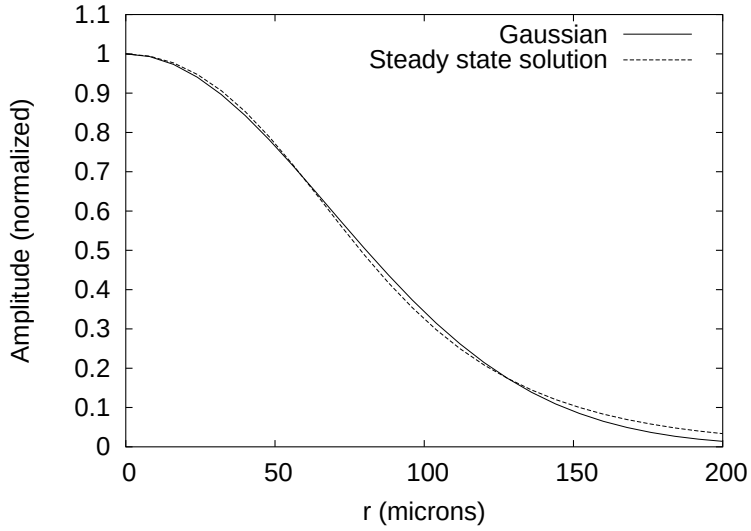

Figure 4.8: Niday's steady state solution. This solution contains a power of roughly 470 MW, and beam width of roughly 97 μm. The peak intensity which defines this solution is 3.2×10^{16} W/m^2. Also shown is a Gaussian profile, with the same peak intensity and width. From reference [23].

is very similar to a Gaussian (Figure 4.8). Thus, the steady state solutions for the field and plasma become

$$\mathcal{E}_0(r,z) = u(r)e^{i\bar{k}z} \tag{4.3}$$

$$\rho_0(r) = \sqrt{\frac{b}{\alpha}}|u(r)|^K, \tag{4.4}$$

respectively, where $\bar{k}$ is an eigenvalue that can be solved for by inserting the above equations back into our propagation equation (4.1). This results in

$$\bar{k} = -\frac{\sigma\omega\tau}{2}\sqrt{\frac{b}{\alpha}}|u(r)|^3 + k_0 n_2|u(r)|^2 = k_0 n_3|u(r)|^3 + k_0 n_2|u(r)|^2. \tag{4.5}$$

المنارة للاستشارات
www.manaraa.com

Now, if we let $\mathcal{E}_+$, $\mathcal{E}_-$, and ρ_+ be small perturbations compared to $\mathcal{E}$ and ρ, then we can investigate a time-perturbed solution of

$$\mathcal{E}(r,z,t) = \mathcal{E}_0(r,z) + \mathcal{E}_+(r,z)e^{-i\Omega t} + \mathcal{E}_-(r,z)e^{i\Omega t}, \tag{4.6}$$

$$\rho(r,z,t) = \rho_0(r) + \rho_+(r,z)e^{-i\Omega t} + \rho_+^*(r,z)e^{i\Omega t}, \tag{4.7}$$

where we have to use ρ_+ and ρ_+^* since the plasma density is real. Following Niday's derivation we obtain

$$\rho_+ = \frac{Kb|\mathcal{E}_0|^{2K-2}\left(\mathcal{E}_0^*\mathcal{E}_+ + \mathcal{E}_0\mathcal{E}_-^*\right)}{2\alpha\rho_0 - i\Omega}, \tag{4.8}$$

$$\rho_+^* = \frac{Kb|\mathcal{E}_0|^{2K-2}\left(\mathcal{E}_0^*\mathcal{E}_- + \mathcal{E}_0\mathcal{E}_+^*\right)}{2\alpha\rho_0 + i\Omega}. \tag{4.9}$$

Next, we insert equations (4.6-4.9) into equation (4.1), expand the terms, and keep only the linear perturbation terms. In this step we must utilize the fact that $K = 3$ for UV ionization in air. We then get

$$\frac{\partial\mathcal{E}_0}{\partial z} = \nabla_\perp^2\mathcal{E}_0 + ik_0n_2|\mathcal{E}_0|^2\mathcal{E}_0 - i\frac{\sigma\omega\tau}{2}\rho_0\mathcal{E}_0, \tag{4.10}$$

for the zero order terms,

$$\begin{aligned}\frac{\partial\mathcal{E}_+}{\partial z} = i\frac{1}{2k}\nabla_\perp^2\mathcal{E}_+ + i\frac{k''}{2}\Omega^2\mathcal{E}_+ + ik_0n_2|\mathcal{E}_0|^2\left[2\mathcal{E}_+ + \mathcal{E}_-^*\right] \\ - i\frac{\sigma\omega\tau}{2}\left(\rho_0\mathcal{E}_+ + \frac{Kb|\mathcal{E}_0|^{2K}}{2\alpha\rho_0 - i\Omega}\left[\mathcal{E}_+ + \mathcal{E}_-^*\right]\right)\end{aligned} \tag{4.11}$$

المنارة للاستشارات
www.manaraa.com

for the terms oscillating as $e^{-i\Omega t}$, and

$$\frac{\partial \mathcal{E}_-}{\partial z} = i\frac{1}{2k}\nabla_\perp^2 \mathcal{E}_- + i\frac{k''}{2}\Omega^2 \mathcal{E}_- + ik_0 n_2 |\mathcal{E}_0|^2 \left[2\mathcal{E}_- + \mathcal{E}_+^*\right] - i\frac{\sigma\omega\tau}{2}\left(\rho_0 \mathcal{E}_- + \frac{Kb|\mathcal{E}_0|^{2K}}{2\alpha\rho_0 - i\Omega}\left[\mathcal{E}_- + \mathcal{E}_+^*\right]\right) \quad (4.12)$$

for the terms oscillating as $e^{i\Omega t}$. These last two equations give the evolution of the coupled perturbation fields $\mathcal{E}_+$ and $\mathcal{E}_-$. We now assume a solution for these perturbation fields of

$$\begin{aligned} \mathcal{E}_+(r,z) &= u_+ \exp(\lambda\, z + i\bar{k}z + i\mathbf{k}_\perp \cdot \mathbf{r}) \\ \mathcal{E}_-(r,z) &= u_- \exp(\lambda^* z + i\bar{k}z - i\mathbf{k}_\perp \cdot \mathbf{r}), \end{aligned} \quad (4.13)$$

where $\mathbf{k}_\perp$ is the transverse wave vector $k_x\hat{x} + k_y\hat{y}$, $\mathbf{r}$ is the transverse coordinate $x\hat{x} + y\hat{y}$, $\bar{k}$ is defined as in equation (4.5), and λ now represents the eigenvalue or growth rate of the field. Substituting these solutions into equations (4.11) and (4.12), defining the contribution from the $\nabla_\perp^2$ as $\bar{k}_\perp \equiv -\frac{\mathbf{k}_\perp^2}{2k}$, and cancelling the exponential dependence gives

$$\begin{aligned} (i\bar{k} + i\bar{k}_\perp + \lambda)u_+ =& iGu_+ - iC\left(\rho_0 u_+ + A(\Omega)\left[u_+ + u_-^*\right]\right) \\ &+ iB\left[2u_+ + u_-^*\right], \end{aligned} \quad (4.14)$$

$$\begin{aligned} (i\bar{k} + i\bar{k}_\perp + \lambda^*)u_- =& iGu_- - iC\left(\rho_0 u_- + A^*(\Omega)\left[u_- + u_+^*\right]\right) \\ &+ iB\left[2u_- + u_+^*\right], \end{aligned} \quad (4.15)$$

المنارة للاستشارات
www.manaraa.com

where

$$A(\Omega) \equiv \frac{Kb|\mathcal{E}_0|^{2K}}{2\alpha\rho_0 - i\Omega} \qquad B \equiv k_0 n_2 |\mathcal{E}_0|^2$$
$$C \equiv \frac{\sigma\omega\tau}{2} \qquad G(\Omega) \equiv \frac{k''}{2}\Omega^2. \tag{4.16}$$

Putting equation (4.14) and the complex conjugate of (4.15) into matrix form, we have

$$i \begin{bmatrix} X & Y \\ -Y & -X \end{bmatrix} \begin{bmatrix} u_+ \\ u_-^* \end{bmatrix} = \begin{bmatrix} i\bar{k} + i\bar{k}_\perp + \lambda & \\ & -i\bar{k} - i\bar{k}_\perp + \lambda \end{bmatrix} \begin{bmatrix} u_+ \\ u_-^* \end{bmatrix}, \tag{4.17}$$

where

$$X(\Omega) \equiv 2B + G(\Omega) - C\left(\rho_0 + A(\Omega)\right) \tag{4.18}$$

$$Y(\Omega) \equiv B - CA(\Omega). \tag{4.19}$$

It is only possible to have a nontrivial solution to this matrix equation if

$$\lambda^2 = Y^2 - (X - \bar{k} - \bar{k}_\perp)^2. \tag{4.20}$$

This factors as

$$\lambda^2 = (B - A(\Omega)C)^2 - \left(2B - A(\Omega)C + G - \bar{k} - \bar{k}_\perp - C\rho_0\right)^2 \tag{4.21}$$

المنارة للاستشارات
www.manaraa.com

From equation (4.5) and equation (4.16) it is easy to infer

$$\bar{k} = B - C\rho_0. \tag{4.22}$$

Substituting this into the equation for λ^2 gives a reduced form of

$$\lambda^2 = \left(2Y - \bar{k}_\perp + G\right)\left(\bar{k}_\perp - G\right). \tag{4.23}$$

To achieve stability, the growth rate, $Re(\lambda)$, needs to be non-positive. When GVD is not included, as in Niday's analysis, this only occurs at zero spatial frequency or zero temporal frequency. This is shown in Figure 4.9 which is a reproduction of a figure from Niday's dissertation and Figure 4.10 which uses the new recombination rate and the higher MPI coefficient of 3.9×10^{-33} m^3/W^2. Both use an intensity of 3.2×10^{16} W/m^2. With these two figures the difference that the new recombination rate makes can be seen in the maximum value of the growth rate and its shape in the $\bar{k}_\perp$ direction.

When GVD is included very little changes until very high temporal frequencies are reached. Figures 4.9 and 4.10 were reproduced with GVD and shown at a higher temporal frequency in Figures 4.11 and 4.12 so the difference is made clear. Comparing these two figures shows how the higher MPI coefficient affects the growth rate. The higher parameter raises the value of the growth rate at higher spatial frequencies. It should be noted that the value of the growth rate

المنارة للاستشارات
www.manaraa.com

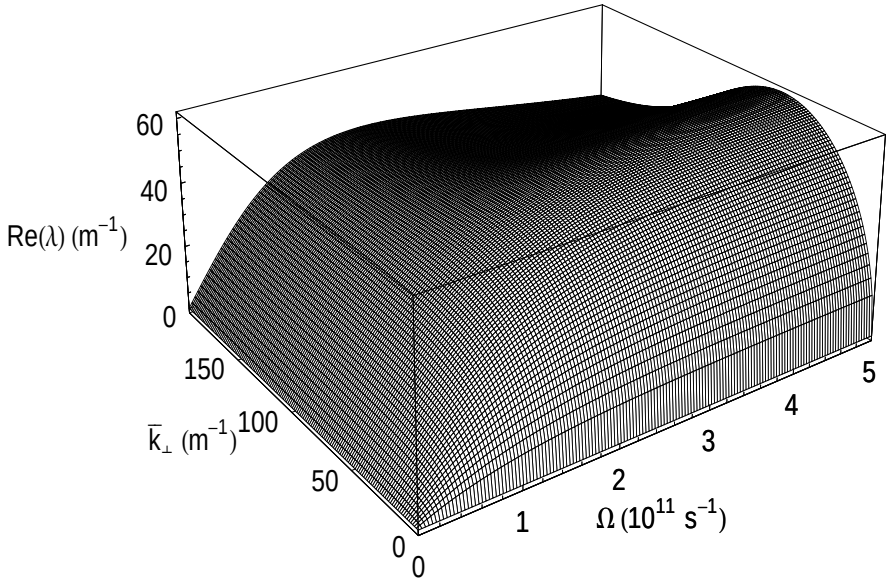

Figure 4.9: Growth rate vs. $\bar{k}_\perp$ and Ω without GVD with the original value for α and $\beta^{(K)}$, for an intensity of 3.2×10^{16} W/m^2. A reproduction of Figure 4.2 in reference [21].

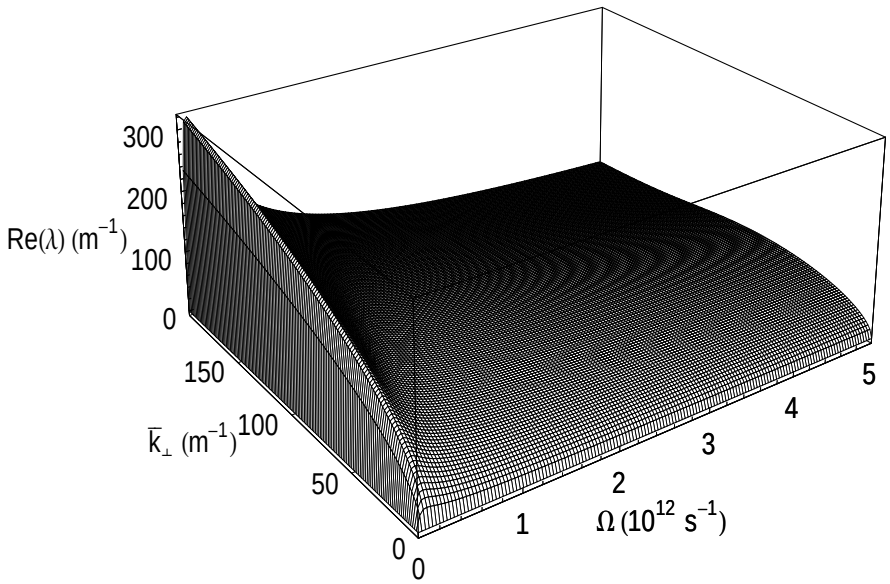

Figure 4.10: Growth rate vs. $\bar{k}_\perp$ and Ω, without GVD, with α_n, and with a higher MPI coefficient, for an intensity of 3.2×10^{16} W/m^2.

المنارة للاستشارات
www.manaraa.com

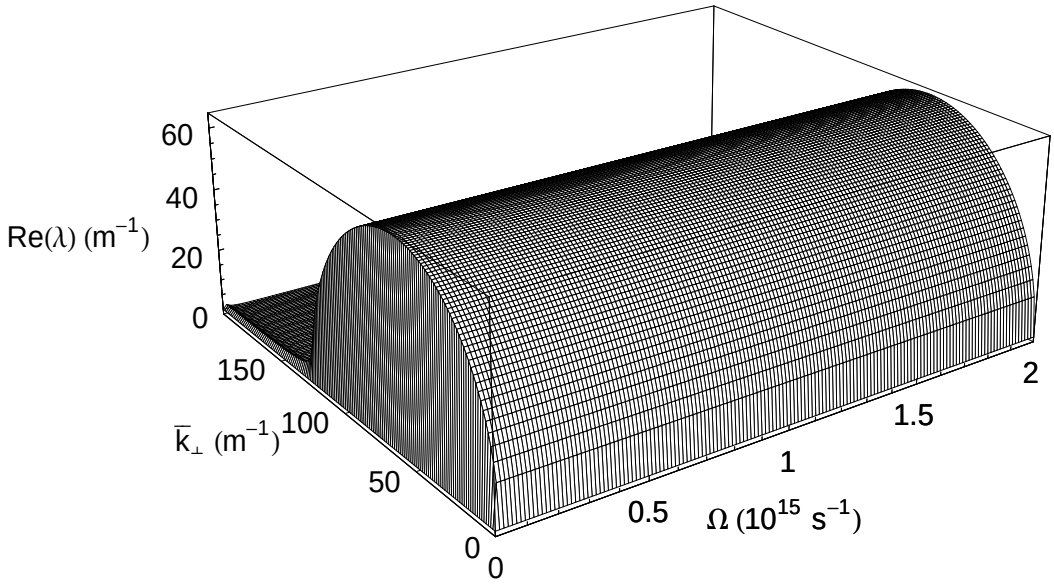

(a) Without GVD

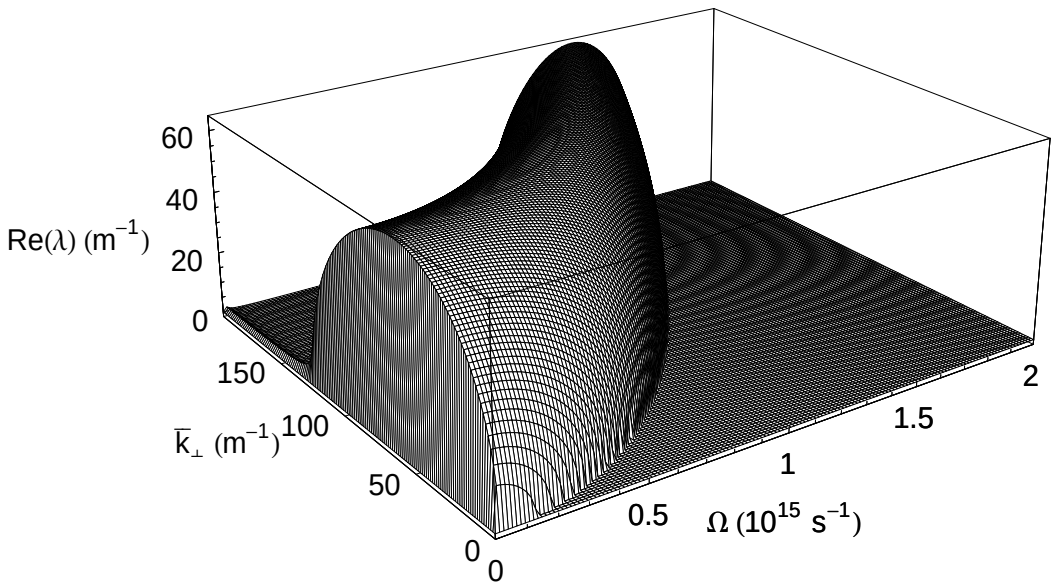

(b) With GVD

Figure 4.11: (a) Figure 4.9 shown at high temporal frequencies. (b) The same figure with the inclusion of GVD.

المنارة للاستشارات
www.manaraa.com

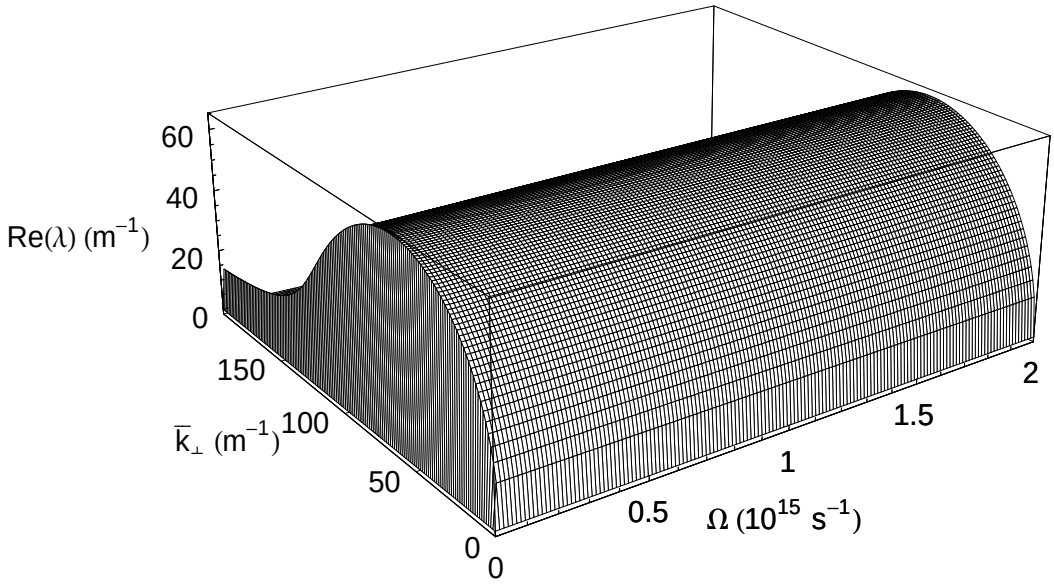

(a) Without GVD

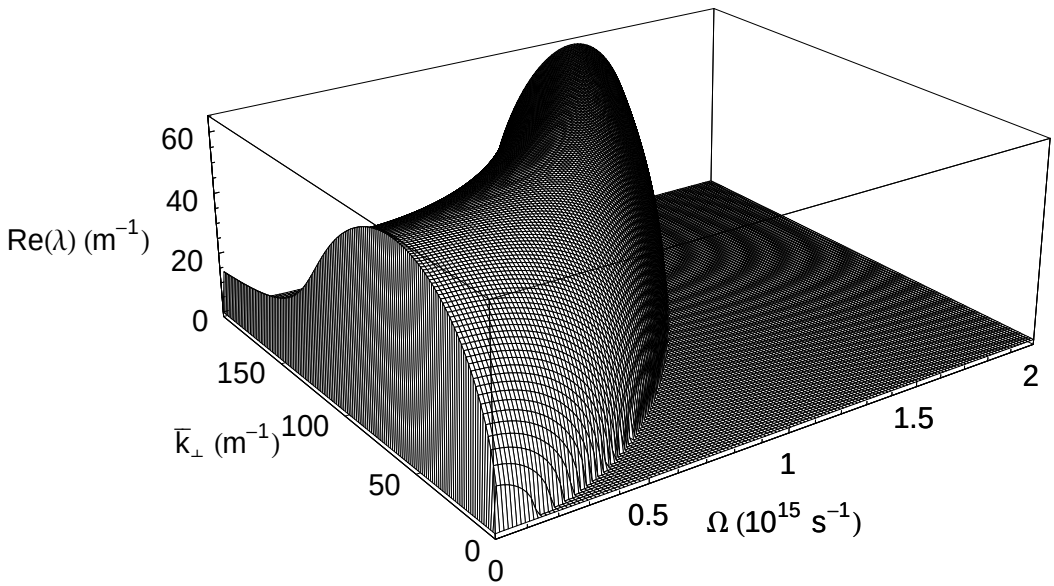

(b) With GVD

Figure 4.12: (a) Figure 4.10 shown at high temporal frequencies. (b) The same figure with the inclusion of GVD.

المنارة للاستشارات
www.manaraa.com

is not zero where it appears to be negligible. Figure 4.13 shows that, with GVD included, the growth rate is non-zero at all non-zero temporal frequencies, even when $\bar{k}_\perp = 0$.

For a closer look at the stability of the propagation of the pulses, let us examine the high frequency limits of the growth rate. As $\bar{k}_\perp \to \infty$,

$$Re(\lambda) \to \pm Im(Y). \tag{4.24}$$

Since Y is not dependent on G, the GVD term, this is the same result that Niday achieved [21]. Thus, there will always be a positive growth rate, although it will be capped for large spatial frequencies. This limit is shown in Figure 4.14 for the new recombination rate, and high MPI coefficient showing the negative root as a dashed line. However, the limit of infinite spatial frequency is never reached because of the paraxial approximation which assumes the transverse wave vector, $\mathbf{k}_\perp$, is small compared to k_z. Since $\bar{k}_\perp$ is related to $\mathbf{k}_\perp$, its maximum value is limited to approximately 3000 m^{-1} for a grid with $\triangle x = 0.8$ mm.

Taking the limit of high temporal frequencies, as $\Omega \to \infty$, the growth rate remains positive without an upper limit. In this case, $Y \to B$, so with GVD included,

$$\lambda^2 \to \left(2B - \bar{k}_\perp + G\right)\left(\bar{k}_\perp - G\right), \tag{4.25}$$

المنارة للاستشارات
www.manaraa.com

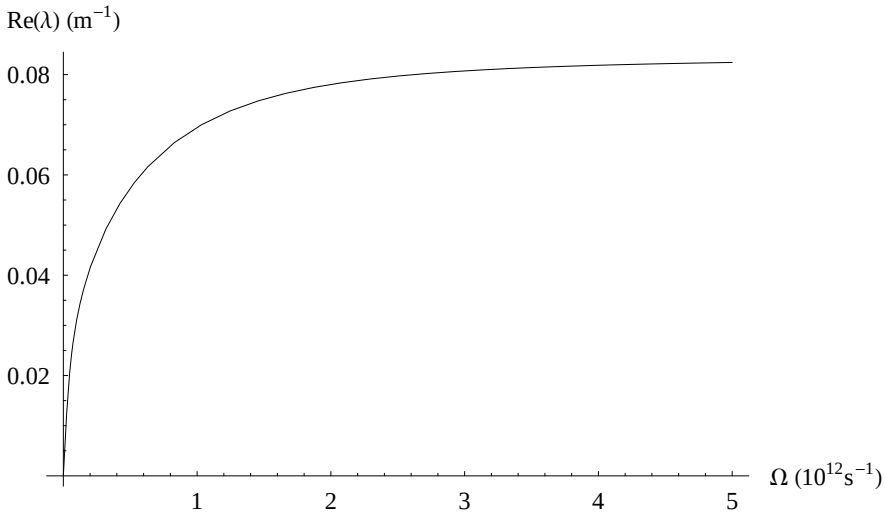

(a) Lower Temporal Frequencies

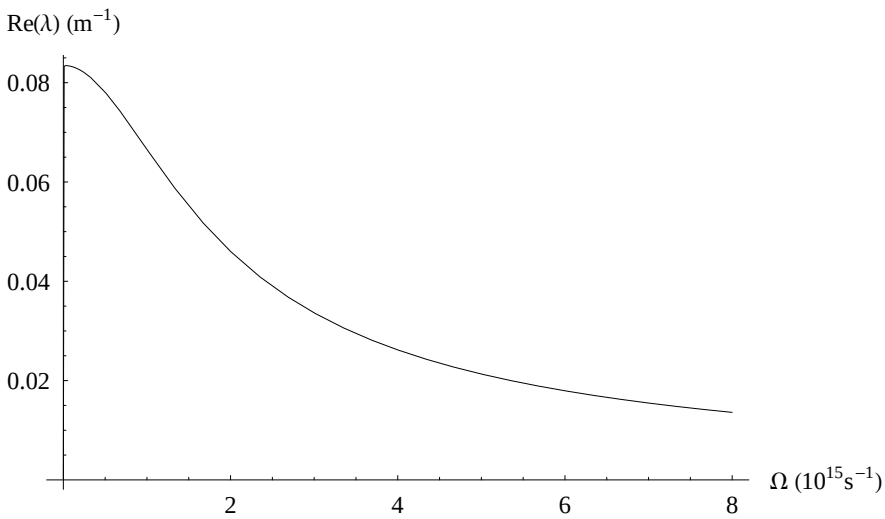

(b) High Temporal Frequencies

Figure 4.13: Growth rate vs. Ω, when $\bar{k}_\perp = 0$ using the parameters in Table 3.1 with α_n and a higher MPI coefficient. (a) Lower temporal frequencies. (b) Higher temporal frequencies where $\lambda = 248$ nm corresponds to 7.6×10^{15} s^{-1}

المنارة للاستشارات
www.manaraa.com

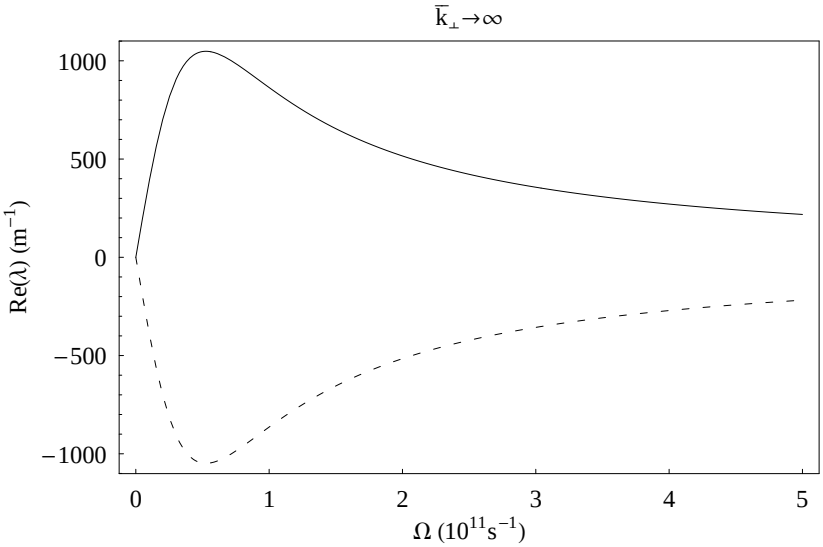

Figure 4.14: Growth rate vs. Ω, when $\bar{k}_\perp \to \infty$ using the parameters in Table 3.1 with α_n. The dashed line is the negative root of the growth rate at this limit.

which leads to an instability region of $G(\Omega) < \bar{k}_\perp < 2B + G(\Omega)$ where the growth rate is positive even as $\Omega \to \infty$. But since G is proportional to Ω^2, this unstable region continually moves to higher values of $\bar{k}_\perp$ and decreases in size. This can be seen in part (b) of Figures 4.11 and 4.12. When not including GVD, there is a constant unstable region of $0 < \bar{k}_\perp < 2B$ as determined in [21], which suggests that difficulties will arise when using numerical techniques for analysis. All of the frequencies present in the numerical model will experience growth, and the growing field will not be bandwidth limited, which is desired for a spectral code. With this in mind, including GVD might suggest that the propagation would be more stable by eliminating the growth of very large temporal frequencies. The results of our simulations, however, reveal breakdown of the collapses after only short propagation distances when GVD is included (shown in a later section).

المنارة للاستشارات
www.manaraa.com

This may be due to the fact that $\bar{k}_\perp = 0$ does not lead to a growth rate of zero, but when GVD is neglected, $\bar{k}_\perp = 0$ does lead to zero growth.

It is clear that in all scenarios, pulse propagation is inherently unstable, with a positive value for the growth rate at all non-zero frequencies. Even if nonlinear losses are considered, such as MPI and plasma loss, compared to the linear loss rate of 2.5×10^{-4} m^{-1}, they are insignificant at low intensities. At intensities corresponding to steady state solutions, the nonlinear loss rate is larger than the linear loss rate at 0.045 m^{-1}. Only when intensities approach 10^{18} W/m^2 does the nonlinear loss rate compare to the unstable growth rate.

Propagation Term Values

In this section, a closer look is taken at each of the individual terms in the propagation equation (2.4) where

$$\begin{aligned}\frac{\partial \mathcal{E}}{\partial z} = &- \frac{ik''}{2}\frac{\partial^2 \mathcal{E}}{\partial t^2} \\ &- \frac{\beta^{(K)}}{2}|\mathcal{E}|^{2K-2}\mathcal{E} \\ &- \frac{\sigma}{2}\left(1 + i\omega\tau\right)\rho\mathcal{E} \\ &ik_0 n_2 |\mathcal{E}|^2 \mathcal{E}\end{aligned} \tag{4.26}$$

will be referred to as the GVD, MPI, plasma, and Kerr terms, respectively. Note that the diffraction term is not listed in this discussion as it applies more to the spatial dimensions versus the temporal dimension. Using the propagation

المنارة للاستشارات
www.manaraa.com

code and Mathematica®, the values of these terms were determined at specific temporal points along the propagation axis (x=0, y=0, t). To understand which terms played a major role in forming the collapse events, the coordinate of the maximum value of the intensity was found. Then, the value of the terms was determined slightly before, at, and slightly after this coordinate. A run with the new recombination coefficient, $N_t = 16384$, and $\triangle t = 0.9$ fs was used in determining these values. A time slice where $x = 0$ of all of these terms is shown in Figures 4.15 through 4.17 at various propagation steps. The units for these terms are the normalized field units per meter. At the beginning of propagation, $z = 2.5$ cm, the first peak has barely started to form at $t = -3.265$ ps. On either side of this peak, $t = -3.355$ ps and $t = -3.175$ ps, there is little difference in the terms. The largest, the plasma term, at 0.101 for the real part increased to 0.117, and the smallest term, the Kerr term, at -10.5123 for the real part increased to -10.5015. The real part of the MPI term was negative and an order of magnitude smaller than the plasma term, and the real part of the GVD term was three orders of magnitude smaller than the plasma. The summation of the Kerr and plasma terms did increase by 0.02 after the peak.

However, after the collapse has had a chance to form at a propagation distance of 15 cm, the behavior of the terms is noticeably different in front of and behind the peak. The peak is now at $t = -4.5$ ps. Just slightly before the peak at $t = -4.52$ ps the real part of the plasma term is -74.43, and slightly after the

المنارة للاستشارات
www.manaraa.com

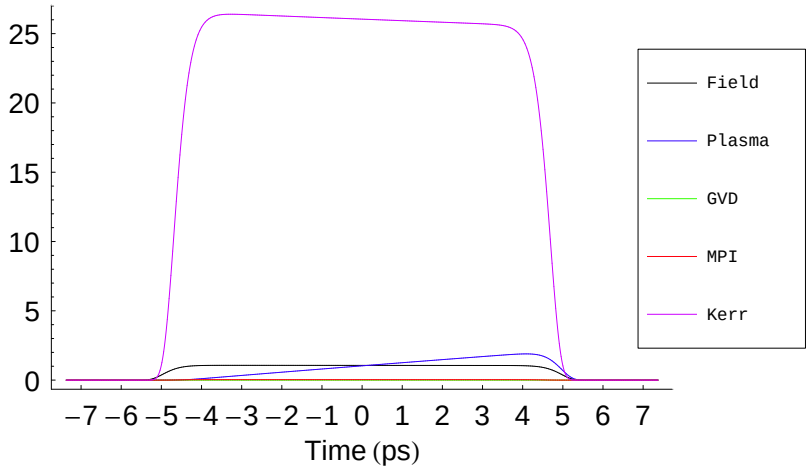

(a)

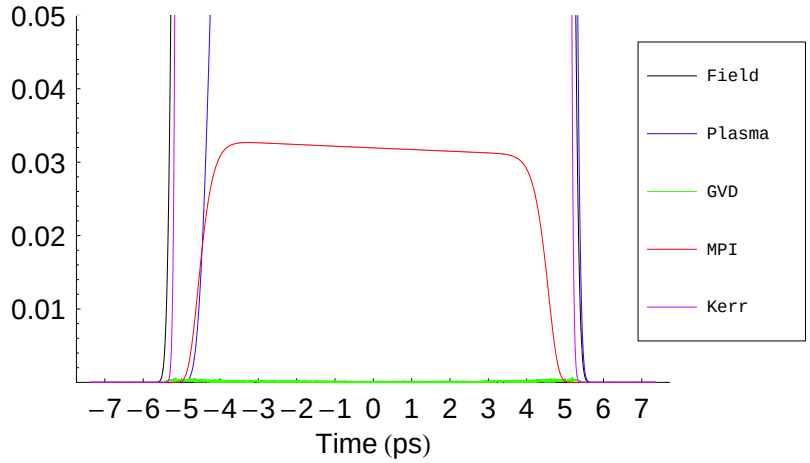

(b)

Figure 4.15: Time slice of the terms in the propagation equation at 2.5 cm. Both a full view (a) and a magnification (b) of the absolute values of each term are shown for a run with the new recombination coefficient and high resolution.

المنارة للاستشارات
www.manaraa.com

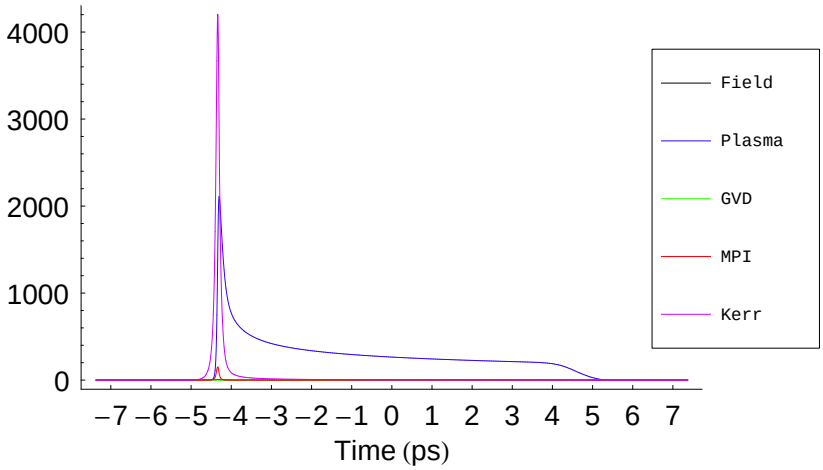

(a)

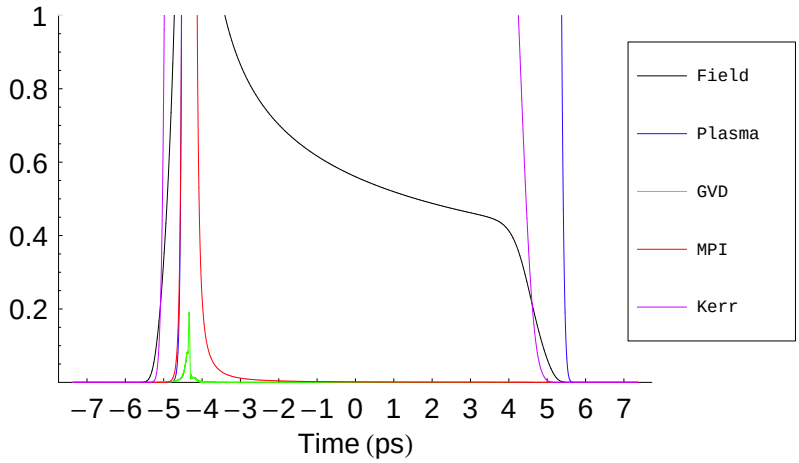

(b)

Figure 4.16: Time slice of the terms in the propagation equation 12.5 cm. Both a full view (a) and a magnification (b) of the absolute values of each term are shown for a run with the new recombination coefficient and high resolution.

المنارة للاستشارات
www.manaraa.com

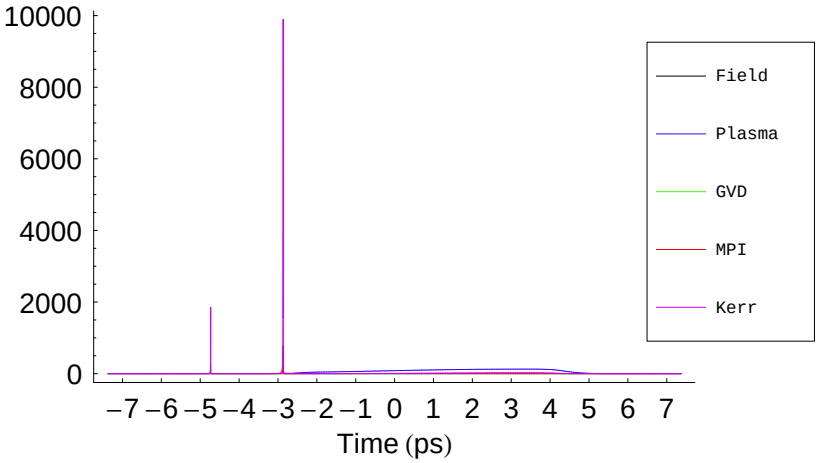

(a)

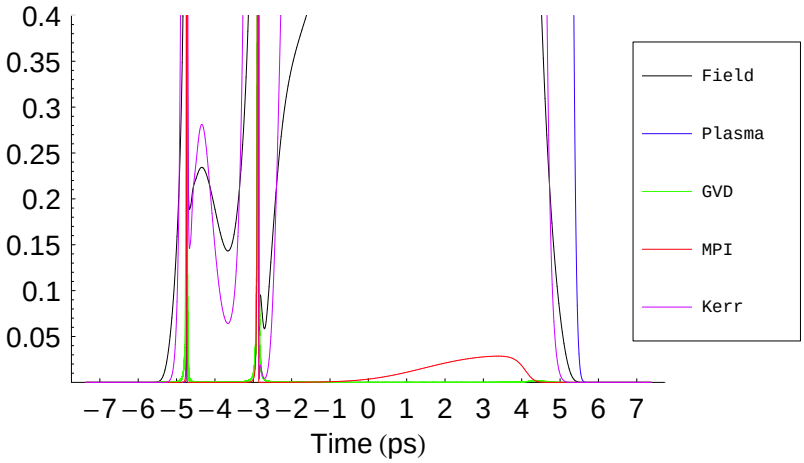

(b)

Figure 4.17: Time slice of the terms in the propagation equation at 50 cm. Both a full view (a) and a magnification (b) of the absolute values of each term are shown for a run with the new recombination coefficient and high resolution.

المنارة للاستشارات
www.manaraa.com

peak at $t = -4.48$ ps it is -1880. However, the real part of the Kerr term only increases from 1170 to 1730 making the summation of the two highly positive before the peak and negative after the peak. This just perpetuates the increasing slope on the front of the collapse and decreasing slope on the back, causing the collapse event to continue to compress temporally. The GVD and MPI terms still remain orders of magnitude smaller than the other terms, thus they do not contribute much to this analysis.

In order to abate this high slope on the front of the pulse, the plasma would need to be higher at the beginning of the pulse. This, however is a difficult task to achieve when working with just one pulse, since the plasma is created after the leading edge of the pulse has passed. This is why studies dealing with multiple pulses is desired. It is suggested that a leading pulse can create a plasma for the following pulse to enter, thus, there is already an established plasma term at the beginning of the pulse that would be able to balance out the Kerr term creating a stable pulse as opposed to a collapse.

As discussed in the section on GVD in Chapter II, group velocity dispersion was included in this study of the collapse events of UV pulses due to the extremely short time scale of the collapses. It was thought that GVD might be able to spread these collapses out, thus curbing their growth and compression. Although adding the GVD term did affect the collapse peaks slightly, it also caused extreme perturbations of the collapses. The nature of the second derivative of the field

المنارة للاستشارات
www.manaraa.com

with respect to time found in the GVD term, is to magnify any noise in the field. A plot of the absolute value of the GVD term for $z = 2.5$ cm is shown in Figure 4.18 revealing the magnification of noise. The GVD parameter, k'' was varied to help determine how much the GVD term affected the pulse propagation code. It was found that the higher the value of k'', the sooner the collapsed peaks showed signs of perturbation. This is shown in Figure 4.19. It displays a magnification of a collapse event of a pulse having the same parameters from Table 3.1, except for k'' being 0, 1.45×10^{-28}, and 1.45×10^{-26} s^2/m with $N_t = 4096$, $\triangle t = 3$ fs. The old value for α is used. Without GVD included, the pulse can propagate to a distance of 75 cm and farther, but when normal GVD is included, perturbations appear at 47.5 cm. For the bigger GVD value, the pulse only gets to 25 cm before it shows signs of perturbations. To avoid these perturbations in the results of the code due to numerical error being magnified, we neglected GVD for many of the simulations.

The terms in the plasma propagation equation (2.5) were also investigated. The diffusion strength D is still assumed to be zero, but the avalanche ionization term is included to check the validity of neglecting it in the main propagation code. The following terms will be referred to as the MPI, recombination and avalanche terms, respectively:

$$C\rho|\mathcal{E}|^2, \qquad \frac{\beta^{(K)}|\mathcal{E}|^{2K}}{K\hbar\omega}, \qquad \alpha\rho^2, \tag{4.27}$$

المنارة للاستشارات
www.manaraa.com

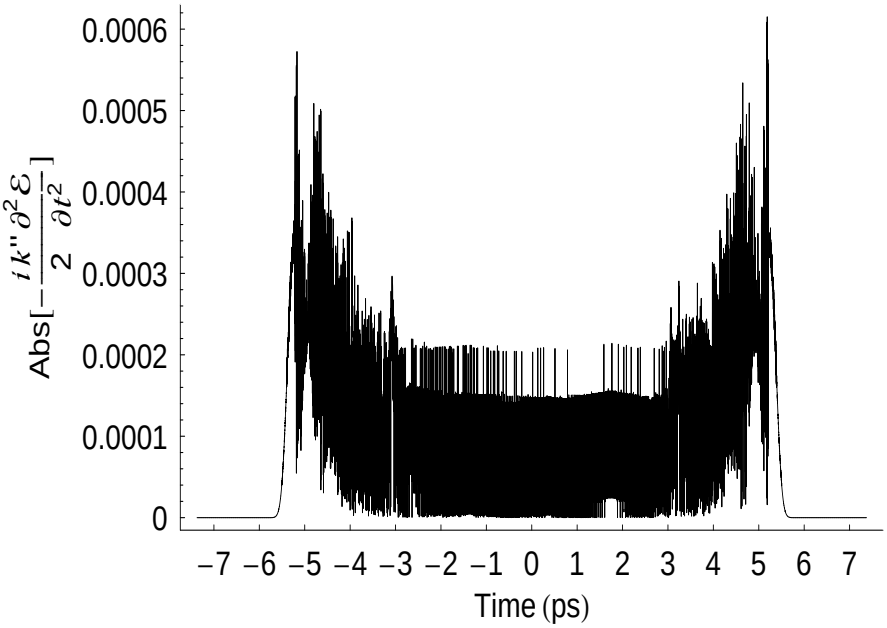

Figure 4.18: A middle slice of the absolute value of the GVD term with respect to time. Shown for the pulse at $z = 2.5$ cm with the new alpha value. Note the perturbations due to taking the second derivative numerically.

where $C = \sigma/E_g$ (assuming a background index of one) and the ionization energy $E_g \approx 11$ eV [22]. As shown in Figure 4.20 the MPI term is much greater than the avalanche term, so this assumption stands.

Experimental Verification

In reference [24], Chalus et al. report experimentally confirming the formation of a filament with the following conditions: power of 500 MW, beam waist of 100 μm, pulse duration of 200 ps. These parameters were used as initial conditions for the propagation code with both a supergaussian time profile and a regular Gaussian profile. The supergaussian temporal shape of the pulse is chosen to simulate the time independent solution assumed by the theory proposed

المنارة للاستشارات
www.manaraa.com

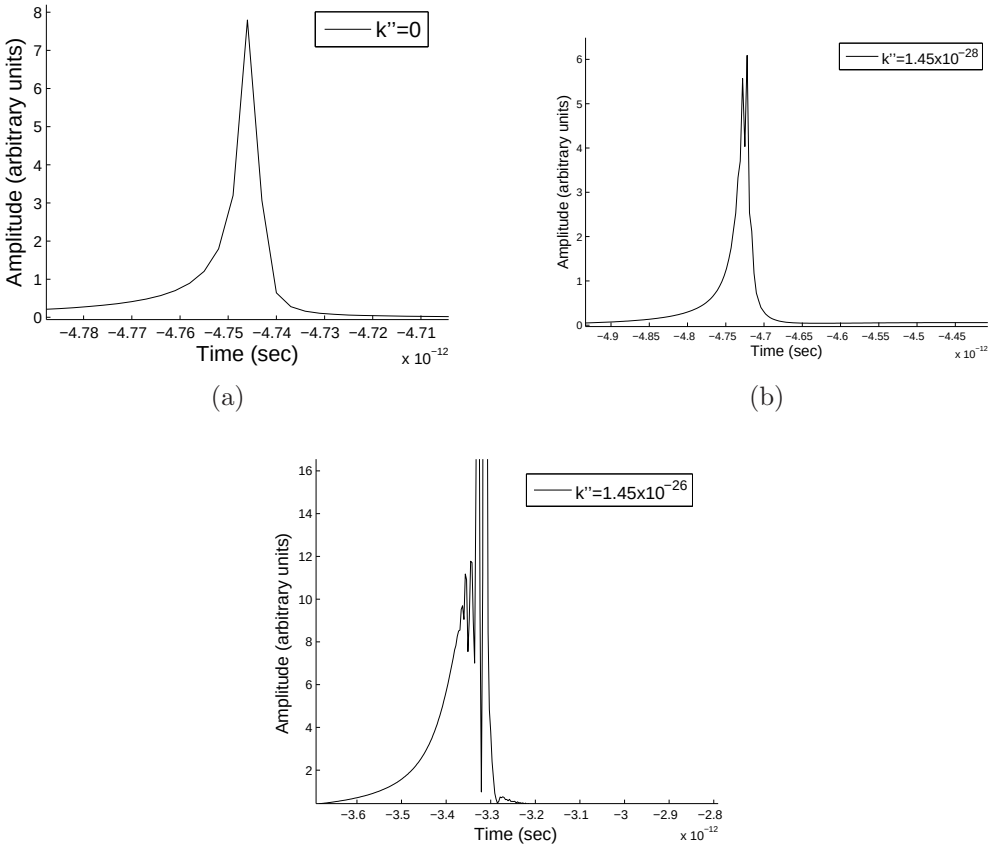

Figure 4.19: Part(a) shows the first collapse of the pulse with no GVD term at $z = 0.75$ m. Part(b) shows the first collapse of the pulse with $k'' = 1.45 \times 10^{-28}$ s^2/m for the GVD term at $z = 0.475$ m. Part(c) shows the second collapse of the pulse with $k'' = 1.45 \times 10^{-26}$ s^2/m for the GVD term at $z = 0.275$ m. The first collapse was already perturbed to such high frequency, aliasing was occurring.

المنارة للاستشارات
www.manaraa.com

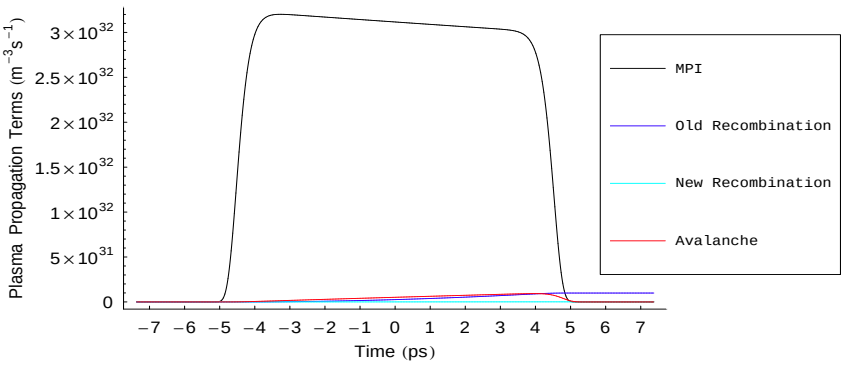

Figure 4.20: A middle slice of the plasma propagation terms with respect to time. Shown for the pulse at $z = 2.5$ cm with both the new and old alpha values.

to explain long distance propagation [11, 21, 23]. The new recombination rate was used as well as the higher MPI coefficient to ensure convergence. The superguassian run resulted in similar collapse events as previously discussed. However, the Gaussian run resulted in the pulse somewhat collapsing, but into only one event that stabilized over the first 70 cm of propagation. It could be able to propagate stably for even longer distances. This could not be determined due to time constraints, however. Figures 4.21 through 4.25 show a 3D representation of this Gaussian pulse as it propagates, along with its k-space form in (a) as well as the fluence profile of the pulse in (b). Figure 4.26 shows a time slice along the x-axis as well as the fluence profile of the same pulse. A larger spatial grid size of $N_x = N_y = 512$ has prevented the fluence profile from showing signs of grid overflow. Note, however, that by 50 cm the pulse is starting to diverge beyond the limits of the spatial grid. The ABC's will not be able to absorb the field as it

المنارة للاستشارات
www.manaraa.com

diverges further off the grid at farther propagation distances. When the fluence profile begins to show signs of this, the results from the propagation code become invalid.

Summary

In summary, time convergence is achieved up to at least 1 m of propagation when a larger value of $\beta^{(K)}$ is used. However, with the original value, convergence can only be achieved up to 25 cm even with $N_t = 16384$ and $\triangle t$=0.9 fs. This prevents a detailed analysis of the collapse events. Only the fact that the collapses increase in intensity and decrease in duration during that first 25 cm can be confirmed. In order to study this further, one would need a code that has adaptable grid parameters to achieve enough resolution of the collapses, yet not overload the computer's ability, or one would need access to a supercomputer. It was shown using a stability analysis that in all cases the pulse remains modulationally unstable. The GVD term specifically introduces instability for all temporal frequencies at $\bar{k}_\perp = 0$. The high temporal frequency limit was taken to reveal the effect that GVD has on the numerical stability, and the high spatial frequency limit revealed the same information as in reference [21]. The second derivative in the GVD term is believed to cause nonphysical perturbations to show in the pulse and collapses after just a short propagation distance during runs including GVD. A closer look at the actual values of the propagation terms revealed that the Kerr and plasma terms interacted to determine the slope of the field. The other terms

المنارة للاستشارات
www.manaraa.com

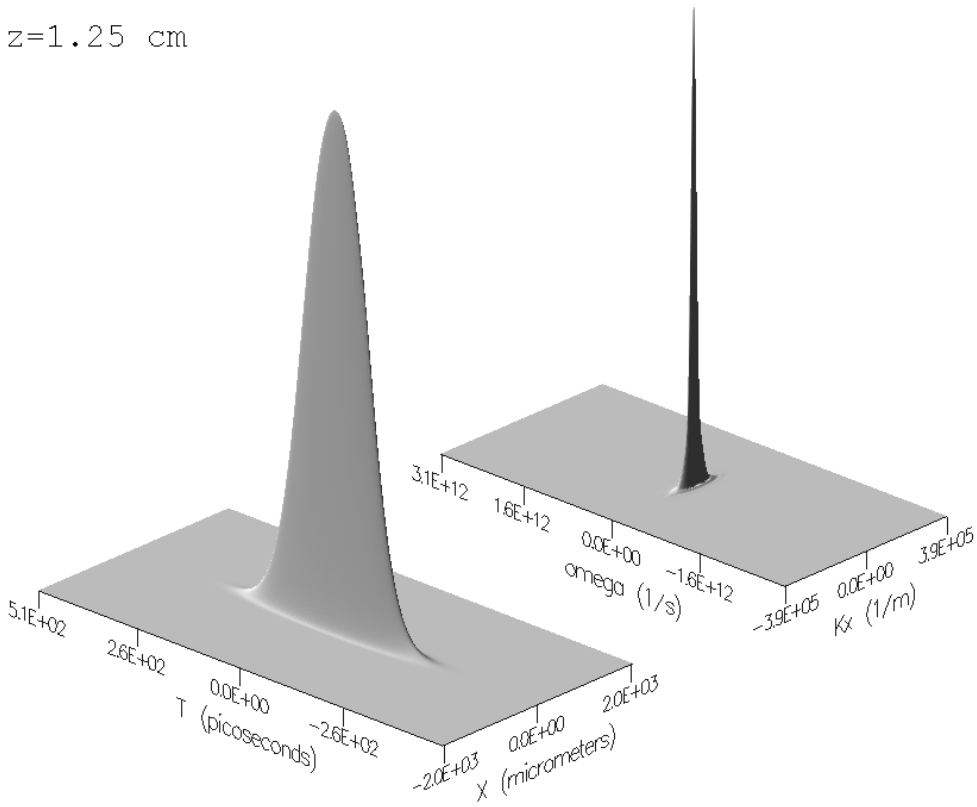

(a)

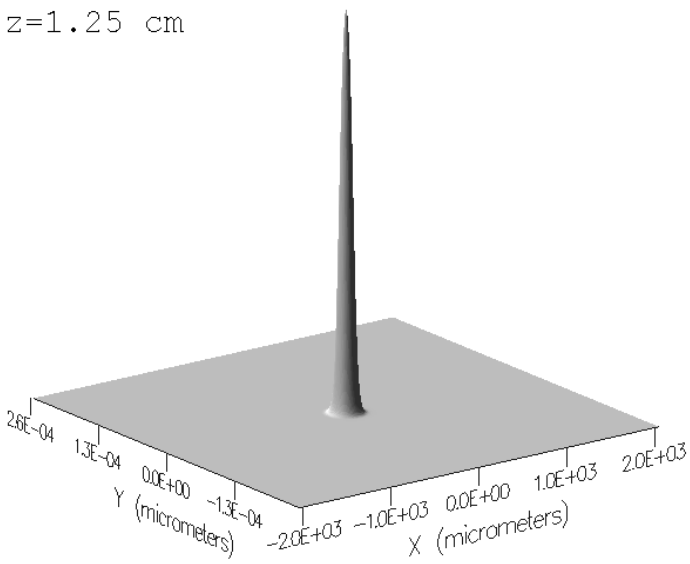

(b)

Figure 4.21: The propagation of a Gaussian 200 ps duration pulse along with its k-space representation. (b)is the fluence profile. The peak amplitude of (a) was normalized to one at $z = 0$, and the following plots are on the same scale. The fluence profiles in the following plots are not to scale.

المنارة للاستشارات
www.manaraa.com

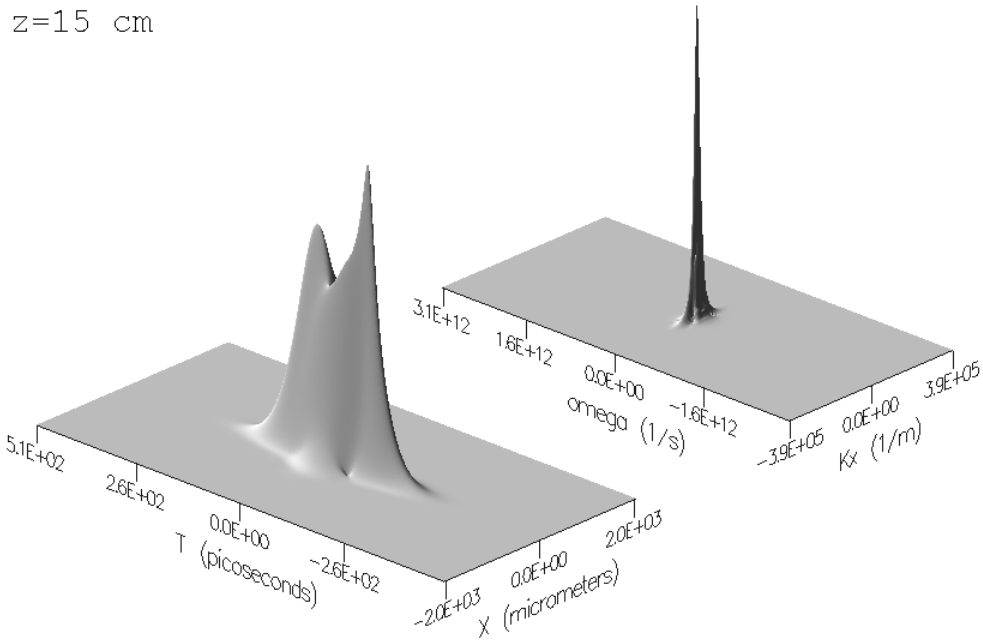

(a)

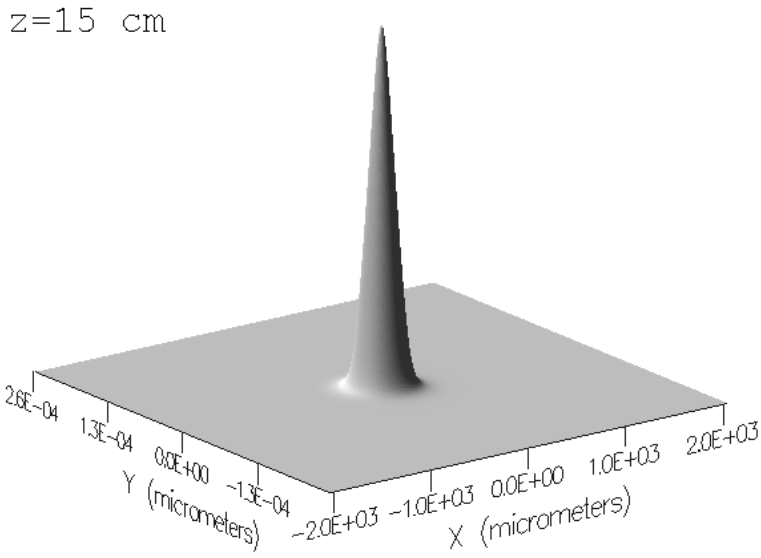

(b)

Figure 4.22: The propagation of a Gaussian 200 ps duration pulse along with its k-space representation. (b)is the fluence profile.

المنارة للاستشارات
www.manaraa.com

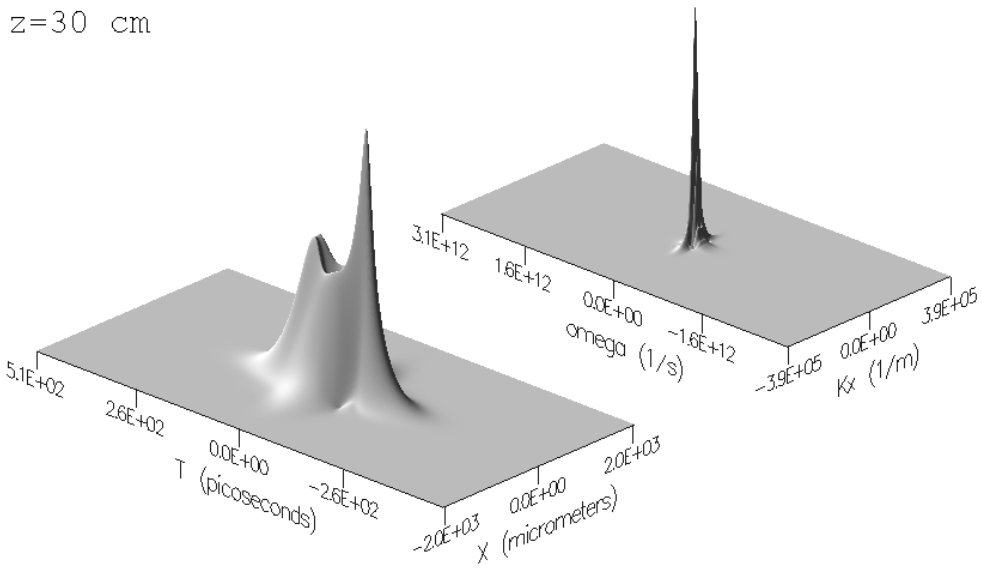

(a)

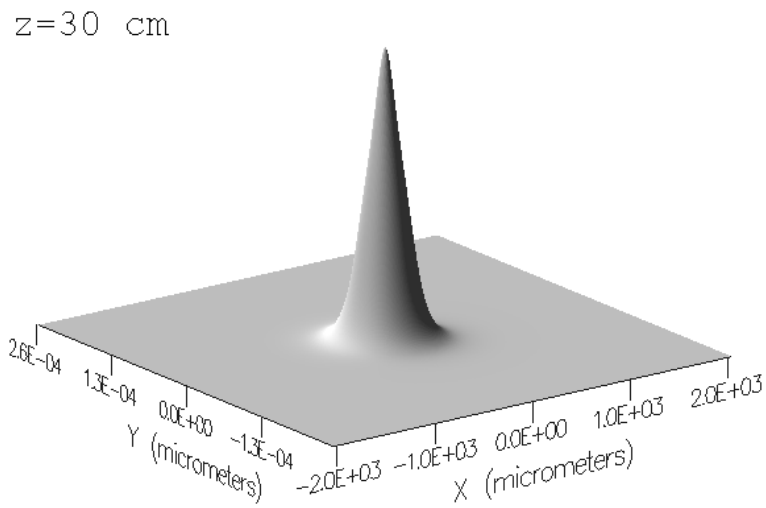

(b)

Figure 4.23: The propagation of a Gaussian 200 ps duration pulse along with its k-space representation. (b)is the fluence profile.

المنارة للاستشارات
www.manaraa.com

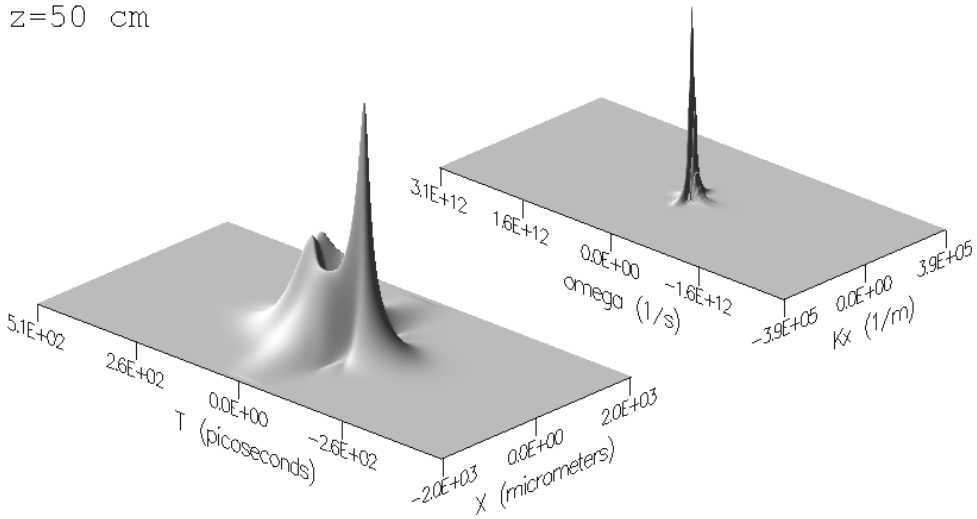

(a)

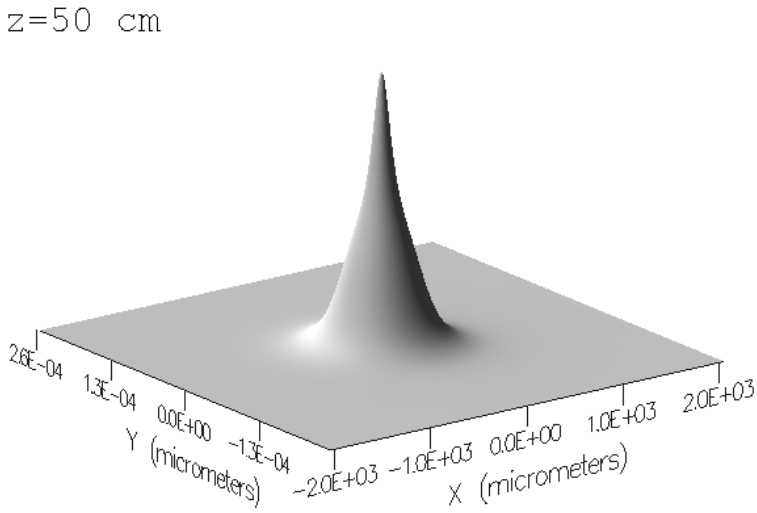

(b)

Figure 4.24: The propagation of a Gaussian 200 ps duration pulse along with its k-space representation. (b)is the fluence profile. Note that the pulse in (a) is starting to spread beyond the limits of the spatial grid. It has not effected the fluence profile, yet.

المنارة للاستشارات
www.manaraa.com

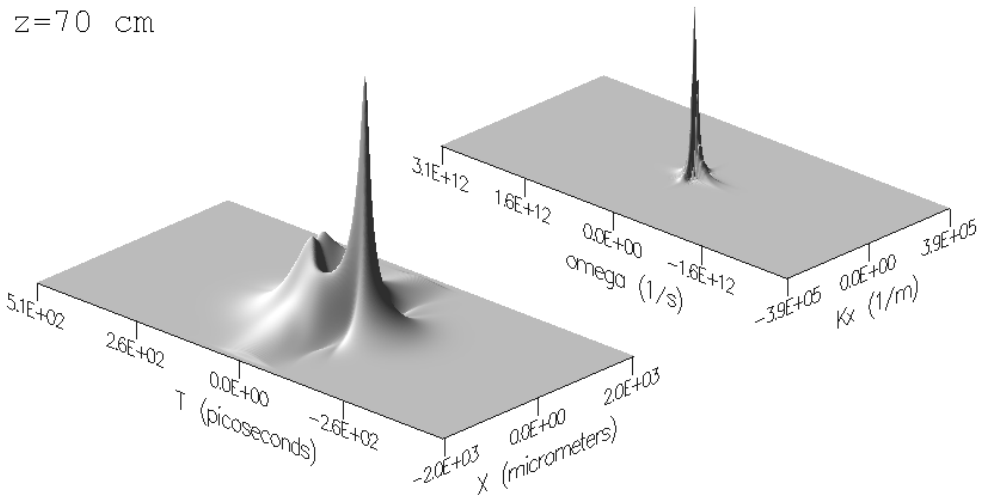

(a)

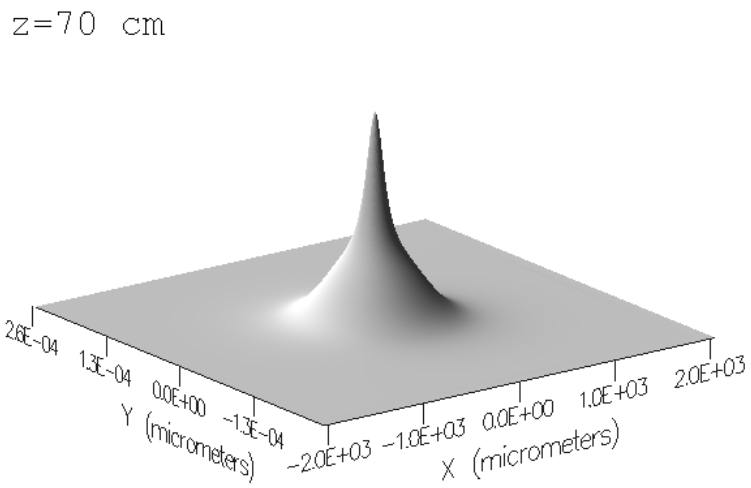

(b)

Figure 4.25: The propagation of a Gaussian 200 ps duration pulse along with its k-space representation. (b)is the fluence profile. Note that the pulse in (a) is continuing to spread beyond the limits of the spatial grid. It still has not effected the fluence profile. Further propagation steps were unavailable due to time constraints.

المنارة للاستشارات
www.manaraa.com

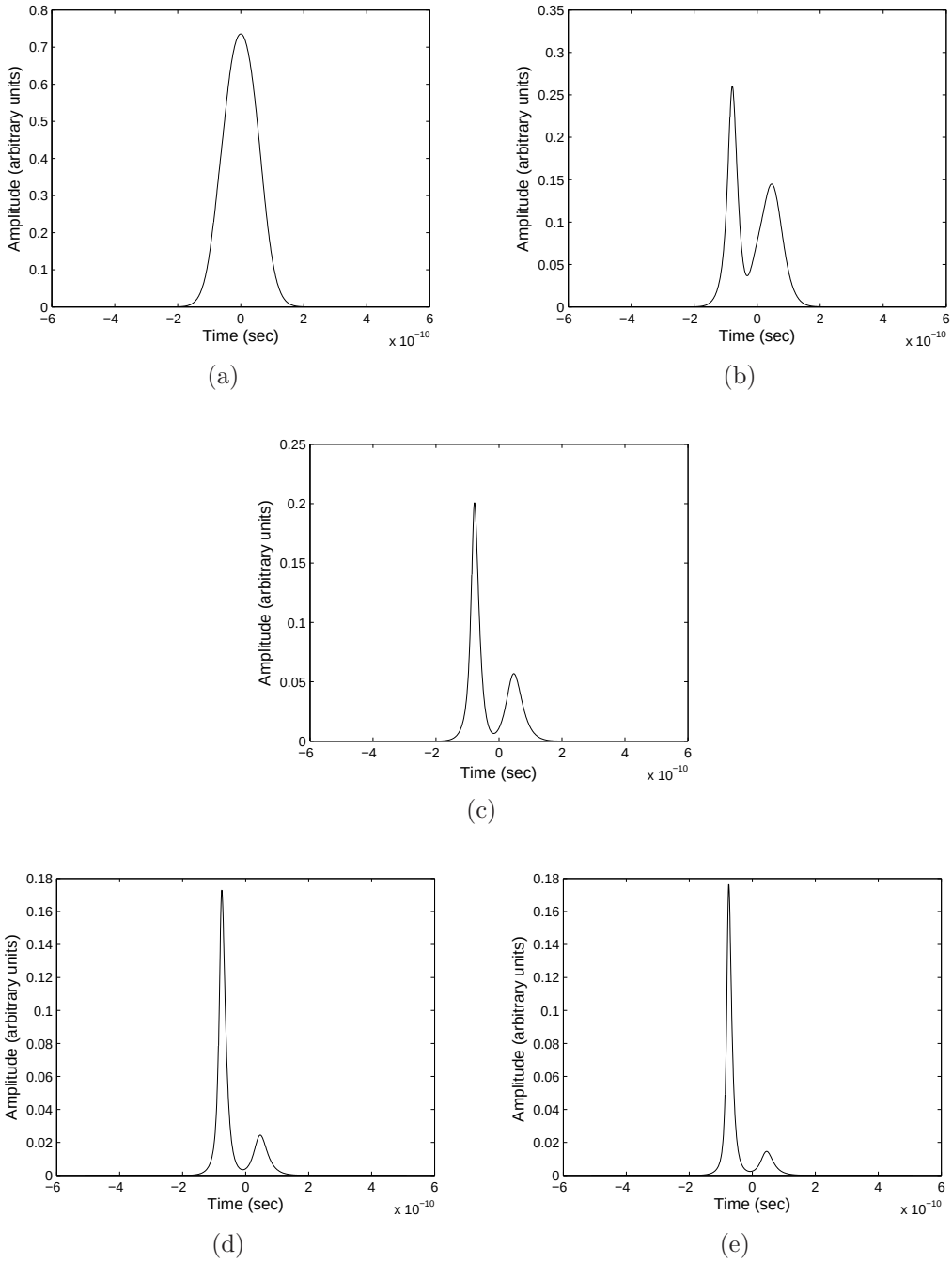

Figure 4.26: A time slice of a Gaussian 200 ps duration pulse at (a) 1.25 cm, (b) 15 cm, (c) 30 cm, (d) 50 cm, and (e) 70 m.

المنارة للاستشارات
www.manaraa.com

were orders of magnitude smaller and therefore contributed little to the evolution of the collapses. It is suggested that if a plasma could be introduced to the front of the pulse, say by a previous pulse, the plasma term could balance out the Kerr term and establish a stable pulse as opposed to collapse events. The terms in the plasma propagation were also examined to confirm the approximation of neglecting avalanche ionization.

المنارة للاستشارات
www.manaraa.com

V. Conclusions and Suggestions

This chapter will discuss the conclusions that can be drawn from the research presented and explains the impact this research has on the scientific investigation of filamentation and future applications for the United States Air Force. It also gives suggestions for future research that can stem off what has been done here.

Research Conclusions

In addition to Niday's research on the modeling of the propagation of long UV pulses, Muller came to several relevant conclusions. First, he established numerical grid parameters in the spatial dimension that accurately displayed the pulse's propagation. He could not, however, establish grid parameters for the time dimension that prevented numerical sampling errors, because the collapses condensed to durations on the order of the smallest grid spacing he was able to attain. Second, he established that the collapses are strongly related to the plasma generated by the pulse. Third, he discovered that the input power of the pulse was directly proportional to the rate at which the collapses formed. Working from this information and the foundation laid by Niday, this work presents several more conclusions on the phenomenon of collapse events forming on the leading edge of a self-focusing UV picosecond pulse.

The first conclusion of this research is that the collapse events become too short in duration for the computational power available to be able to handle the numerical parameters needed to achieve convergence of these events. Convergence

المنارة للاستشارات
www.manaraa.com

was only demonstrated for the first 25 cm of propagation before the collapses condensed to a duration unable to be represented by a grid spacing of 0.9 fs. This initial convergence confirms that at least the formation of the collapses is being appropriately represented by the numerical code, even if their complete evolution remains a mystery. Complete time convergence was achieved up to 1 m, however, using a MPI coefficient 10 times larger than originally specified. This larger value causes the losses to overcome the increasing intensity of the collapse so the numerical parameters are able to represent it longer before it eventually compresses to a duration on the order of our grid spacing. This confirms that the collapses continue to decrease in duration, but do not continually increase in intensity, at least with this higher MPI loss.

The second conclusion established in this research stems from the investigation of the individual propagation term values. The ever increasing front slope of the collapse is due to the Kerr term dominating the plasma term. The decreasing negative slope on the trailing edge of the collapse is due to the plasma term decreasing greatly while the Kerr term only increases slightly. The other terms in the propagation equation are orders of magnitude smaller than these two terms. This interaction suggests that if more plasma is present at the front of the pulse, the plasma term will be more negative, possibly allowing for a more neutral slope of the leading edge of the pulse, establishing stable propagation of the pulse as opposed to the collapse events being generated.

المنارة للاستشارات
www.manaraa.com

Third, it was concluded that GVD, although affecting the collapses slightly due to their short duration, can be neglected. The nature of the GVD term induces an unbounded growth of all frequencies introduced by the numerical code. By including GVD in the analysis, any and all noise is amplified causing nonphysical perturbations in the results for propagation. The fact that the value of the GVD term in the propagation term investigation was insignificant compared to the Kerr and plasma terms and the results of the stability analysis lead to this conclusion.

Another conclusion of this study also stems from the stability analysis. It was discovered that linear instability is inherent in the propagation of UV pulses with the initial conditions specified in this study. Even zero spatial frequencies have a positive growth rate when GVD is included. Losses were found to compare to this growth rate only at high intensities on the order of 10^{18} W/m^2. This is found to be true with all combinations of the original and new values for the recombination rate and the MPI coefficient.

Finally, the initial conditions of an experiment that generated filamentation was introduced to the propagation code using the new recombination rate and a higher MPI coefficient. This run generated only one collapse event that stabilized and continued to propagate farther than 1 m. However, results after 30 cm start to exhibit signs that at least part of the pulse has spread beyond the limits of the spatial grid, introducing numerically induced phenomena.

المنارة للاستشارات
www.manaraa.com

Impact of Research

The study of the filamentation of UV light is extremely relevant to the United States Air Force. If we can understand the intricate details behind how light filaments are able to travel long distance without excessive dispersion, diffraction or even annihilation due to obscurants, our ability to harness this phenomenon for numerous applications is greatly increased. By modeling filamentation accurately, the ideal initial conditions can be determined that promote desired effects for applications such as remote sensing of aerosols in the atmosphere, protection of equipment and personnel from lighting strikes, or the ability to direct energy at certain targets for their destruction. Niday's UV propagation model is a piece of this understanding. Using it to investigate the behavior of how light travels and the nonlinear effects that counteract normal diffraction, we are one step closer to the realization of these beneficial applications to the Air Force.

By achieving time convergence of the pulse propagation up to a certain distance, we are able to confirm that the results presented here are not due to numerical error, but accurately represent the behavior of the model. However, until the model accurately represents experimental data, we must search for the right initial conditions or a better model. The numerical error, found by previous research, of collapse events occurring rapidly on the trailing edge after some distance of propagation has been eliminated. The benefit of this convergence and elimination of numerical error is validation of further results involving the intrica-

المنارة للاستشارات
www.manaraa.com

cies of propagation. The failure of convergence at further distances also points out the need for an adaptable grid size or supercomputer that can achieve even more resolution of the collapses as they continue to intensify and shorten in duration.

Having a more in depth analysis of the GVD parameter provides several benefits to the continued analysis of UV propagation. The stability analysis revealed that including GVD brought stability in the high temporal range, but also brought instability in the low spatial range, which could be the cause of additional perturbations in the pulse during propagation. By combining the understanding of why fragmentation of the collapses occurs in relation to GVD and the realization that GVD does not play a big enough role to curb the time shortening of the collapse events, we can neglect GVD in future research dealing with relatively long pulses. This simplifies the propagation equation for easier analysis and manipulation.

The results of the investigation on the values of each of the propagation terms allow future research to focus on the terms which play the biggest roles in the formation of these collapse events. The interaction of these terms, Kerr and plasma, determined the sign of the slope of the field. Knowing this suggests that having a preceding pulse that establishes a higher plasma term at the front of the pulse could lead to the elimination of the collapse events that occur on the leading edge of the pulse.

المنارة للاستشارات
www.manaraa.com

The stability analysis done in this research shows that with GVD considered and all combinations of recombination rates and MPI coefficients, there is still unstable growth for all spatial and temporal frequencies. This is valuable in that it raises the question of whether we have correct values for all of our parameters or if filamentation is even theoretically possible with the model assumed for these simulations. Possibly, filamentation could arise from the instability itself. With the knowledge of this instability we are one step closer to finding the answers to the filament phenomenon.

With the simulation of the propagation of a pulse imitating one that experimentally created a filament, the code produced only one collapse event that was able to converge. The results of this run could be consistent with the experimental results, thereby validating the propagation code. If this is indeed the case, attention can turn toward the conditions needed to produce these results as opposed to determining the details of the non-successful runs. However, the numerical grid size still limited these results.

Suggestions for Further Research

Because of the time limitation on this research, there are many areas in the long range propagation of UV laser pulses that have been left unaddressed. This research has also raised many new questions that should be answered about the interaction of self-focusing, diffraction, and other losses. Further expansion of Niday's propagation model is needed to be able to fully grasp the concepts of

المنارة للاستشارات
www.manaraa.com

UV filamentation and to better represent the unknown intricacies of leading edge collapse events. Experimental verification is also needed to be done alongside this theoretical modeling work in order to confirm its results.

Expansions to the current propagation model could involve inclusion of certain terms that were neglected for simplification. One of these terms is the last term in equation (2.2), the Raman effect. Including this scattering turns n_2 into a non-instantaneous self-focusing term by introducing a time dependence part according to

$$ik_0 n_2 |\mathcal{E}|^2 \mathcal{E} \rightarrow ik_0(1-f)n_2|\mathcal{E}|^2\mathcal{E} + ik_0 f n_2 \left[\int_{-\infty}^{\infty} dt' R(t-t')|\mathcal{E}(t')|^2\right]\mathcal{E}(t) \quad (5.1)$$

where f is the fraction of the Kerr effect which is not instantaneous, but delayed due to stimulated molecular Raman scattering. Diffusion, D in the plasma equation (2.5), could also be included by making it nonzero. Another way to expand the code for better propagation is to add Rayleigh scattering once greater distances are achieved. This would attenuate the power of the beam with respect to propagation distance by

$$\frac{dP}{dz} = -\beta^{(K)}\frac{1}{w^4}P^3 - n_0\beta_4\frac{1}{w^3}P^{5/2} - \alpha_R P, \quad (5.2)$$

where the first term on the right hand side is the power attenuation through the photon ionization, the second represents plasma absorption, and the third is the

المنارة للاستشارات
www.manaraa.com

power loss through Rayleigh scattering. For a wavelength of 248 nm, $\alpha_R = 5\times10^{-4}$ m^{-1} [17]. If propagating distances of kilometers, one could also add variation to the background index of refraction n_0, introducing dependence on turbulence, altitude, and so forth.

Another improvement to the model code that would aid in the study of the leading edge collapse events is to introduce a variable time step. By being able to use a larger $\triangle t$ where the pulse is fairly stable, but at the same time use a very small time step only where the collapse events are occurring, one could keep the grid size at a reasonable level while still achieving high resolution in the critical areas. It could be implemented by basing the time step on the derivative of the field itself instead of being a constant input by the user. If the derivative of the field is small, $\triangle t$ can be larger, but where the derivative is large, the time step would be decreased allowing for more resolution at the collapses. Further thought is needed to consider how the grid size would be determined for this variable time step. This adaptation to the code would allow for much better resolution while requiring less time and memory to compute. This higher resolution could lead to more insight as to the nature of these collapse events. However, the FFT could no longer be taken in the time dimension since it requires a fixed time step. This is possible if GVD is not considered in the equation. Another option to increase resolution, but also avoid the numerical error introduced by the limited grid sizes, is to run the code on supercomputers. This could be the key to bridging the gap

المنارة للاستشارات
www.manaraa.com

between experimental results and the results produced numerically with the 3D propagation code.

More detailed study of each collapse event could also be done by taking a collapsed section of a pulse that has been propagated by the original code and using it as an input to a higher resolution propagation code. The higher resolution would have to be interpolated from the less frequent data points of the original run. Care would have to be taken to extract the collapse event from the original run before it has collapsed to a size that the grid can no longer accurately represent so that the interpolated higher resolution points will be correctly determined. With this idea, one could see if these individual collapse events are able to propagate by themselves after splitting from the pulse.

The introduction of obscurants to the pulse path could be another extension of this propagation model. By zeroing out a portion of the field at a particular propagation step, an obscurant can be simulated. Studies could be done to see how certain pulses overcome or are dissipated by this obstruction. Experiments could be done on different sizes and transparencies of the simulated barriers, as well as how placement affects the outcome. Does placing the obstruction on axis or off, or at the beginning of propagation or after collapse events have already been allowed to form make a difference in the pulse being able to continue to propagate? All of these scenarios would help in understanding the self-healing properties of filaments.

المنارة للاستشارات
www.manaraa.com

Because the plasma density is not immediately terminated at the end of the pulse, but dies down slowly, the idea of introducing multiple pulses to the code is intriguing. Would there be enough left over plasma that would interact with the next laser pulse causing a completely different effect than was seen with the first pulse? Maybe the plasma would just cause an increase or decrease in the effects presented in this study. After many pulses have been propagated, the interaction of them could lead to steadier reaction of the following pulses eliminating the leading edge collapses. Enough questions are raised when thinking about pulse interactions to warrant an investigation.

The idea that X-waves could be a representation of filaments propagating long distances is an exciting and promising idea. Research could be done to investigate how X-waves could relate to these collapse events found on the leading edge of pulses being propagated with the model presented here. Studies could be done on what conditions would be necessary to allow these collapses to form into X-waves. An X-wave could also be used as an initial input to study how the simulation allows it to propagate. Once a true X-wave is able to propagate without undergoing diffraction or dispersion, slight variations could be made to the input pulse to deviate from the ideal conditions to see if the deviations could be overcome as the pulse propagates to form this X-wave.

More experimental data is needed with regard to longer UV pulses at high powers. The successes and failures of these experiments could help guide following

المنارة للاستشارات
www.manaraa.com

research to the areas that are most feasible and applicable to UV radiation. An extension of the stability analysis that includes nonlinear terms could also be conducted to determine if stability is established when higher order terms are considered. Also, a more in depth loss analysis could be done.

Further studies could be done with regard to the needs of the Air Force in the area of UV long distance propagation. A survey could be done to determine the specific areas that deal with remote sensing, laser induced and guided lightning, or directed energy applications in which the military is particularly interested. From this, one could receive guidelines for wavelengths, powers, and other specifications required for use in combat to use as initial conditions in simulations.

Finally, more runs should be made with the initial conditions described in the experiment of reference [24] to include larger spatial grid sizes or higher ABC's to alleviate the restriction of the pulse due to numerical limitations. Also, the wavelength could be changed from 248 nm to 266 nm as was used in the experiment. If these runs are indeed successful in creating a filament that can propagate long distances, by starting with this scenario, small changes can be made to pinpoint exactly what is causing the code to exhibit the multiple non-convergent collapses whether it be grid size, values of the recombination rate or MPI coefficients, or the initial shape of the pulse.

المنارة للاستشارات
www.manaraa.com

Bibliography

1. P. Rairoux, H. Schillinger, S. Niedermeier, M. Rodriguez, F. Ronneberger, R. Sauerbrey, B. Stein, D. Waite, C. Wedekind, H. Wille, L. Woste, and C. Ziener. Remote sensing of the atmosphere using ultrashort laser pulses. *Applied Physics B: Lasers and Optics*, 71(4):573–580, 2000.

2. Dennis R. Alexander and Mark L. Rohlfs. Femtosecond laser pulse propagation through aerosol clouds. In *2002 IEEE International Geoscience and Remote Sensing Symposium (IGARSS 2002)*, volume 5, pages 2631–2633, Toronto, Ont., Canada, Jun 24-28 2002. Dept. of Electrical and Engineering, Center for Electro-Optics, University of Nebraska, Lincoln, NE 68588-0511, United States, Institute of Electrical and Electronics Engineers Inc.

3. S. Skupin, L. Berge, U. Peschel, and F. Lederer. Interaction of femtosecond light filaments with obscurants in aerosols. *Physical Review Letters*, 93(2):023901–1, 2004.

4. J. Davis, R. E. Terry, G. M. Petrov, and A. L. Velikovich. Alternate approaches to laser guided discharges. Technical Report NRL/MR/6720–06-8956, 19 APR 2006.

5. Jens Schwarz and Jean-Claude Diels. Uv filaments and their application for directed energy. In *Laser and Beam Control Technologies*, volume 4632, pages 122–133, San Jose, CA, United States, Jan 21-23 2002 2002. University of New Mexico, 800 Yale Blvd. NE, Albuquerque, NM 87131, United States, The International Society for Optical Engineering.

6. Patrick Rambo, Jens Schwarz, Luca Giuggioli, and Jean-Claude Diels. Long gap laser-induced discharges using a femtosecond uv source. *Conference on Quantum Electronics and Laser Science (QELS) - Technical Digest Series*, page 147, 2000.

7. P. Rambo, J. Schwarz, and J. C Diels. High-voltage electrical discharges induced by an ultrashort-pulse uv laser system. *Journal of Optics A: Pure and Applied Optics*, 3(2):146–158, 2001.

8. Paul L. Muller. A study of collapse events in ultraviolet light filaments due to transient edge effects. Master's thesis, Graduate School of Engineering, Air Force Institute of Technology (AETC), Wright-Patterson AFB OH, December 2006. AFIT/GAP/ENPG/06-12.

9. A. Couairon and L. Bergé. Light filaments in air for ultraviolet and infrared wavelengths. *Physical Review Letters*, 88(13):135003, Mar 2002.

المنارة للاستشارات
www.manaraa.com

10. Daniel F. Gordon, Antonio C. Ting, Ilya Alexeev, Richard P. Fischer, and Phillip Sprangle. Direct measurements of the dynamics of self-guided femtosecond laser filaments in air. *IEEE Transactions on Plasma Science*, 34(2):249–253, 2006.

11. Jens Schwarz and Jean-Claude Diels. Analytical solution for uv filaments. *Physical Review A.Atomic, Molecular, and Optical Physics*, 65(1):13806–1, 2002.

12. A. Couairon and A. Mysyrowicz. Femtosecond filamentation in transparent media. *Physics Reports*, 441(2):47–189, 03 2007.

13. Jens Schwarz and Jean-Claude Diels. Long distance propagation of uv filaments. *Journal of Modern Optics*, 49(14):2583–2597, 2002.

14. G. Méjean, J. Kasparian, J. Yu, E. Salmon, S. Frey, and J.-P. Wolf. Multifilamentation transmission through fog. *Phisical Review E*, 72(2):026611–1, 2005.

15. I. Alexeev, A. C. Ting, D. F. Gordon, J. R. Penano, P. Sprangle, and E. Briscoe. Ultraviolet light generation by intense laser filaments propagating in air. In *2005 Conference on Lasers and Electro-Optics, CLEO*, volume 1, pages 189–191, Baltimore, MD, United States, May 22-27 2005. Plasma Physics Division, Naval Research Laboratory, Washington, DC 20375, United States, Optical Society of America, Washington, DC 20036-1023, United States.

16. J. Kasparian, M. Rodriguez, G. Mejean, J. Yu, E. Salmon, H. Wille, R. Bourayou, S. Frey, Y. B Andre, A. Mysyrowicz, R. Sauerbrey, J. P Wolf, and L. Woste. White-light filaments for atmospheric analysis. *Science*, 301(5629):61–64, 2003. Compilation and indexing terms, Copyright 2007 Elsevier Inc. All rights reserved.

17. Hua Zhang. The propagation dynamics of ultraviolet light filament with rayleigh scattering in air. *Chinese Physics*, 14(10):2019–2025, 2005.

18. James T. Murray, Olivier Chalus, and Jean-Claude Diels. High-power uv source for filamentation in air. volume 5707, pages 317–324. SPIE, April 27, 2005 2005.

19. J. C Diels, R. Bernstein, K. E. Stahlkopf, and Xin Miao Zhao. Lightning control with lasers. *Scientific American (International Edition)*, 277(2):50–5, 08 1997.

20. M. Rodriguez, R. Sauerbrey, H. Wille, L. Woste, T. Fujii, Y. B Andre, A. Mysyrowicz, L. Klingbeil, K. Rethmeier, W. Kalkner, J. Kasparian, E. Salmon, J. Yu, and J. P Wolf. Triggering and guiding megavolt discharges by use of laser-induced ionized filaments. *Optics Letters*, 27(9):772–774, 2002.

المنارة للاستشارات
www.manaraa.com

21. Thomas Andrew Niday. *Stability and Transient Effects in Ultraviolet Filaments*. Ph.D. dissertation, Graduate College of the University of Arizona, September 2004. XCAFIT/EN (XCAFITEN).

22. Jens Schwarz, Patrick Rambo, Jean-Claude Diels, Miroslav Kolesik, Ewan M. Wright, and Jerry V. Moloney. Ultraviolet filamentation in air. *Optics Communications*, 180(4):383–390, 2000.

23. Thomas A. Niday, Ewan M. Wright, Miroslav Kolesik, and Jerry V. Moloney. Stability and transient effects in nanosecond ultraviolet light filaments in air. *Physical Review E*, 72(1):016618, July 2005.

24. Olivier Chalus, Alexey Sukhinin, Alejandro Aceves, and Jean-Claude Diels. Propagation of non-diffracting intense ultraviolet beams. *CLEO Post Deadline*, 2007. University of New Mexico, Albuquerque, New Mexico 87131.

25. J. R. Peñano, P. Sprangle, P. Serafim, B. Hafizi, and A. Ting. Stimulated raman scattering of intense laser pulses in air. *Physical Review E*, 68(5):56502–1, 2003.

26. Joseph T. Verdeyen. *Laser Electronics*. Prentice Hall, Englewood Cliffs, NJ, 1994.

27. Eric Weisstein. Eric weisstein's world of physics. *http://scienceworld.wolfram.com/physics/CauchysFormula.html*, 2005.

المنارة للاستشارات
www.manaraa.com

Vita

Teresa Jelaine Fondren was born in Little Rock, Arkansas and grew up in Hot Springs, AR. She graduated as valedictorian from Second Baptist Christian School now called Crossgate Christian Academy. She earned a Bachelor of Science in Physics and Mathematics from the United States Air Force Academy as a distinguished graduate, earning the Outstanding Basic Science student award and becoming a Second Lieutenant in the Air Force. While at Tinker AFB, she received the Company Grade Officer of the Quarter award for the Oklahoma City Air Logistics Center working as the Program Manager for the AF Oil Analysis Program. During her stay in Oklahoma she pinned on First Lieutenant and was accepted into the Air Force Institute of Technology where she pursued her Masters of Science in Applied Physics.

المنارة للاستشارات
www.manaraa.com

REPORT DOCUMENTATION PAGE

Form Approved
OMB No. 074-0188

The public reporting burden for this collection of information is estimated to average 1 hour per response, including the time for reviewing instructions, searching existing data sources, gathering and maintaining the data needed, and completing and reviewing the collection of information. Send comments regarding this burden estimate or any other aspect of the collection of information, including suggestions for reducing this burden to Department of Defense, Washington Headquarters Services, Directorate for Information Operations and Reports (0704-0188), 1215 Jefferson Davis Highway, Suite 1204, Arlington, VA 22202-4302. Respondents should be aware that notwithstanding any other provision of law, no person shall be subject to an penalty for failing to comply with a collection of information if it does not display a currently valid OMB control number.
PLEASE DO NOT RETURN YOUR FORM TO THE ABOVE ADDRESS.

1. REPORT DATE *(DD-MM-YYYY)*	2. REPORT TYPE	3. DATES COVERED *(From – To)*
13-03-2007	Master's Thesis	Jan 2007 – Oct 2007

4. TITLE AND SUBTITLE

Time Resolution of Collapse Events During the Propagation of Ultraviolet Light Filaments

5a. CONTRACT NUMBER

5b. GRANT NUMBER

5c. PROGRAM ELEMENT NUMBER

6. AUTHOR(S)

Fondren, Teresa J., First Lieutenant, USAF

5d. PROJECT NUMBER

5e. TASK NUMBER

5f. WORK UNIT NUMBER

7. PERFORMING ORGANIZATION NAMES(S) AND ADDRESS(S)

Air Force Institute of Technology
Graduate School of Engineering and Management (AFIT/EN)
2950 Hobson Way, Building 640
WPAFB OH 45433-8865

8. PERFORMING ORGANIZATION REPORT NUMBER

AFIT/GAP/ENP/08-M03

9. SPONSORING/MONITORING AGENCY NAME(S) AND ADDRESS(ES)

AFOSR/NE Dr. Arje Nachman (703) 696-8427
875 N. Randolph Rd
Ste 325 Rm 3112
Arlington, VA 22203

10. SPONSOR/MONITOR'S ACRONYM(S)

11. SPONSOR/MONITOR'S REPORT NUMBER(S)

12. DISTRIBUTION/AVAILABILITY STATEMENT

APPROVED FOR PUBLIC RELEASE; DISTRIBUTION UNLIMITED.

13. SUPPLEMENTARY NOTES

14. ABSTRACT

Long distance propagation, or filamentation, of short, intense laser pulses is possible through the balance of two effects: self-focusing, when a nonlinear index of refraction of air is indused by high intensisties, and de-focusing, due to the plasma created by the pulse. Applications for filamentation include areas such as remote sensing and directed energy. A split-step spectral propagation simulation is used to model the behavior of a high intensity ultraviolet laser pulse propagating through air. Convergence of femtocecond duration collapses that form on the leading edge of the pulse in the time domain is achieved with an increase in the multi-photon ionization coefficient. Through an analysis of the relative sizes of each term in the propagation equation, a lack of plasma present at the leading edge of the pulse is found to cause these collapses. Results for a more recent value of the electron—positive ion recombination rate are compared to results from a higher value used in previous work. A linear stability analysis shows inherent instability of the pulses in all cases. The inclusion of group velocity dispersion is shown to increase stability at high temporal frequencies except at zero spatial frequencies. A run similar to an experiment claiming UV filamentation is shown to be artificially limited by numerical parameters.

15. SUBJECT TERMS

Filaments, ultraviolet lasers, wave propagation, self-focusing, nonlinear, numerical analysis, recombination rate, multi-photon ionization, ultrashort pulses

16. SECURITY CLASSIFICATION OF:			17. LIMITATION OF ABSTRACT	18. NUMBER OF PAGES	19a. NAME OF RESPONSIBLE PERSON
a. REPORT	b. ABSTRACT	c. THIS PAGE			T. A. Niday, Maj, USAF
U	U	U	UU	110	19b. TELEPHONE NUMBER *(Include area code)* (937) 255-6565, ext 4828 (Thomas.niday@afit.edu)

Standard Form 298 (Rev. 8-98)
Prescribed by ANSI Std. Z39-18

المنارة للاستشارات
www.manaraa.com